
Article:
Sridhar, R., Che, Y., Phornthepkasemsant, P. et al. (2026) Low-carbon self-compacting glass fiber-reinforced concrete using calcium sulpho-aluminate cement and recycled concrete fine aggregate. ENGINEERING Structure and Civil Engineering, 20 (4). pp. 845-868. ISSN: 3091-5031

https://doi.org/10.1007/s11709-026-1300-1

Low-Carbon Self-Compacting GRC Using Calcium Sulpho-Aluminate Cement and Recycled Concrete Fine Aggregate

Radhika Sridhar[1], Yanfei Che [2], Patraphorn Phornthepkasemsant[3], Thanongsak Imjai[3,*], Elhem Ghorbel[4] and Kypros Pilakoutas[5]

[1] School of Engineering and Technology, Walailak University, Nakhon Si Thammarat, 80161, Thailand
[2] Zhejiang Construction Industry Research Institute Co. Ltd, Baoye Group, China
[3] Department of Civil Engineering, Faculty of Engineering, Burapha University, Chonburi 20131, Thailand
[4] CY Cergy Paris University – 5 Mail Gay Lussac – Neuville sur Oise- 95031 Cergy Paris University, France.
[5] Department of Civil and Structural Engineering, The University of Sheffield, Sheffield, S1 3JD, UK.

*Correspondence: thanongsak.im@eng.buu.ac.th

Abstract

This study presents the development and comprehensive evaluation of low-carbon self-compacting glass fibre-reinforced concrete (GRC) utilizing calcium sulpho-aluminate (CSA) cement and recycled concrete fine aggregate (RFA), targeting enhanced sustainability and durability for high-performance infrastructure applications. Through rigorous mix design optimization, the research demonstrates that substituting natural sand with RFA in CSA cement-based matrices yields a compressive strength of up to 55 MPa after 28 days, comparable to or exceeding conventional mixes, while increasing elastic modulus by approximately 15%, resulting in a stiffer, denser composite. Flexural performance tests revealed that CSA and RFA with GRC achieves a modulus of elasticity of 17 GPa and a modulus of rupture of 3.77 kN, coupled with substantial toughness and ductility, particularly under loads. After 75 days of accelerated ageing, RFA-GRC retained 50 to 70% of its initial MOR and 20 to 40% of STF, outperforming traditional GRC by about 30%, confirming its superior long-term durability. Environmental analysis verifies a dramatic reduction in carbon footprint of CSA RFA GRC achieves up to 74% less CO_2 emissions and 48% lower embodied energy than OPC controls, with values as low as 275 kg CO_2/m^3 and 675 MJ/m^3. Practical validation through prototype drainage channels and permanent formwork further underscores the material's viability, demonstrating excellent workability, structural integrity, and crack resistance. Furthermore, the test results establish CSA and RFA with GRC as a highly sustainable, resilient alternative, supporting circular construction and long-life design in aggressive environments.

Keywords: Low-carbon concrete; Self-compacting concrete; Glass fibre reinforced; Calcium sulpho-aluminate cement; Recycled fine aggregates; Durability enhancement.

1. Introduction

The construction industry is a significant contributor to global carbon emissions, with cement production alone responsible for approximately 7% of global anthropogenic CO_2 emissions [1]. The environmental impact of conventional concrete, particularly due to the high energy demand and CO_2 emissions associated with the production of Ordinary Portland Cement (OPC), has prompted the search for sustainable alternatives. One promising material that has gained attention in recent years is calcium sulpho-aluminate (CSA) cement, which offers a more environmentally friendly option for concrete production due to its lower calcination temperature and reduced clinker content compared to OPC [2]. CSA cement has the potential to reduce CO_2 emissions significantly, making it a key player in the development of low-carbon concrete solutions [3].

Self-compacting concrete (SCC) has become an essential advancement in concrete technology, offering substantial benefits in terms of workability, efficiency, and ease of placement, particularly in areas with dense reinforcement [4-6]. SCC eliminates the need for mechanical vibration during casting, reducing labour costs and ensuring better flowability and finish quality, especially in complex formworks [7]. However, despite the widespread adoption of SCC, the incorporation of CSA cement into SCC formulations, particularly with glass fibre reinforcement (GRC) and recycled concrete aggregates (RCA), remains underexplored [8]. This gap in knowledge presents a significant opportunity for researchers to investigate the synergistic effects of these materials on both the sustainability and performance of self-compacting concrete [9]. The lack of comprehensive studies that combine CSA cement, RCA, and GRC in self-compacting concrete formulations highlights a critical research gap in the field of sustainable construction materials [10-11].

GRC is known for its superior mechanical properties, such as enhanced tensile and flexural strength, improved post-cracking behaviour, and corrosion resistance [12]. These properties make GRC ideal for a wide range of applications, including precast elements, facade panels, and tunnel linings [13]. The inclusion of glass fibres helps to mitigate the brittle nature of conventional concrete, making it more durable and resilient [14]. Despite these advantages, the use of glass fibres in self-compacting concrete systems can be

problematic due to the challenges of fibre agglomeration and the impact on flowability. However, the expansive nature of CSA cement, which promotes the rapid formation of ettringite and other hydration products, has shown promise in improving fibre-matrix bonding and reducing microcracking, thus enhancing the durability of the final product [15]. This innovative approach of integrating CSA cement with glass fibre reinforcement presents a unique opportunity to enhance the performance of self-compacting concrete, overcoming the limitations of traditional formulations and advancing the material's sustainability and durability.

In addition to CSA cement and GRC, the incorporation of recycled fine aggregates (RFA) into concrete formulations presents a valuable opportunity for sustainability. RFA, derived from crushed concrete waste, can reduce the demand for virgin aggregates, contributing to waste reduction and conserving natural resources [16]. However, the use of RFA typically results in lower compressive strength and durability due to the presence of old cement paste that weakens the bond between the aggregates and the cement matrix [17]. Nevertheless, when RFA is combined with alternative binders such as CSA cement, studies have shown that the performance of the recycled concrete can be significantly improved, resulting in concrete that is both environmentally friendly and high performing [18]. The combination of CSA cement, RFA, and glass fibres thus represents a promising new direction for developing sustainable, durable concrete that has yet to be fully explored. The increasing demand for sustainable construction materials has prompted researchers to explore the synergy between CSA cement, RCA, and glass fibre reinforcement in the development of low-carbon self-compacting concrete. CSA cement's unique chemical composition, which includes belite (C_2S), facilitates the rapid formation of strong hydration products that enhance early-age strength and durability [19]. This, in turn, can improve the performance of concrete containing RFA, which is typically weaker than concrete made with virgin aggregates. The combination of CSA cement, RFA, and glass fibres can lead to concrete with superior durability and strength, while also reducing the carbon footprint associated with construction materials [20].

Moreover, the integration of self-compacting properties into concrete made with CSA cement and RFA are particularly advantageous for complex construction projects where high-performance materials are required

[21]. Self-compacting concrete offers improved flowability, ease of placement, and a more uniform finish compared to traditional vibrated concrete, especially in areas with congested reinforcement. By incorporating RFA into these self-compacting systems, the environmental impact of construction can be further minimized, providing a sustainable solution for the growing demand for infrastructure globally [21-23]. The significance of this research lies in its potential to provide a sustainable alternative to conventional concrete, simultaneously enhancing the material's mechanical properties and long-term durability, particularly in demanding environments [24].

Research on the long-term durability of concrete made with CSA cement and RFA have demonstrated improved resistance to common forms of concrete deterioration, including sulphate attack, carbonation, and chloride-induced corrosion [25]. CSA-based concrete exhibits superior resistance to sulphate attack and carbonation compared to conventional OPC concrete, making it ideal for applications in aggressive environments such as coastal regions, industrial zones, and areas subject to high carbonation levels [25]. Furthermore, CSA cement's lower alkalinity enhances the bond between fibres and the matrix, contributing to a more durable material that can withstand long-term exposure to harsh conditions [26].

The use of predictive models has become essential for optimizing the mix design and evaluating the long-term durability of low-carbon self-compacting concrete made with CSA cement and RFA [27]. These models incorporate variables such as CSA content, fibre dosage, and RCA percentage, allowing for a more accurate prediction of concrete performance under various exposure conditions [28]. By utilizing multivariable regression techniques, these models can help engineers design concrete mixes that not only meet the required performance standards but also minimize environmental impact over the lifespan of the structure [29].

The primary objectives of this research are to: (i) investigate the effect of CSA cement on the performance of self-compacting concrete incorporating RFA, (ii) evaluate the impact of glass fibre reinforcement on the strength and durability of these mixes, (iii) develop predictive models to assess the long-term performance of these low-carbon concrete formulations under various exposure conditions, and (iv) develop proof-of-concept applications using the developed mix with CSA, RFA, and glass fibres, such as drainage channels

and permanent formwork, to demonstrate the real-world potential of the material. These objectives aim to address the research gap in integrating CSA cement, RFA, and glass fibres in self-compacting concrete formulations. The novelty of this research lies in its comprehensive approach to optimizing mix design while evaluating the synergistic effects of these materials on both the environmental and mechanical properties of concrete. The development of low-carbon self-compacting GRC using CSA cement and RFA offers significant benefits in sustainability, performance, and durability. This innovative approach not only reduces the environmental impact of concrete production but also enhances the material's strength, durability, and suitability for a wide range of construction applications. As global demand for sustainable construction materials continues to grow, CSA-based GRC presents a promising solution to reduce carbon emissions and improve the performance of infrastructure in aggressive environments. Future research should focus on refining mix designs, expanding the use of predictive durability models, and exploring additional real-world applications for this material in construction projects.

2. Experimental programme

2.1 Materials selection and development of CSA with RFA

For the development of low-carbon self-compacting GRC, a combination of OPC, CSA, super-classified pulverised fuel ash (SPFA), and vitreous calcium aluminosilicate (VCAS) pozzolans were selected. OPC, sourced from cement manufacturer and conforming to BIS EN 197-1 [30], served as the control binder throughout the experimental program. Two types of CSA cements were used: low alkalinity (LA) and rapid hardening (RA), both manufactured by sintering limestone, bauxite, and anhydrite at moderate temperatures (~1300–1350°C). These cements are primarily composed of phases such as ye'elimite (C_4A_3S) and belite (C_2S), which contribute to rapid strength gain and enhanced durability. CSA cement is a more environmentally friendly alternative to OPC, producing significantly lower CO_2 emissions due to its lower production temperature and reduced clinker content. SPFA, is a Class F pozzolanic material [31] that was sourced from Africa and meets ASTM C311 standards [32]. It is highly reactive and widely used as a supplementary material to improve concrete's workability and durability. VCAS pozzolans, produced from waste E-glass fibres, were mixed with lime and alumina, melted, rapidly quenched, and finely ground. This

material is highly reactive, contributing to improved hydration and durability in cementitious systems. These materials, selected for their low-carbon characteristics and enhanced performance, were used to optimize the mix design for producing a sustainable and durable concrete suitable for high-performance applications in aggressive environments. The chemical compositions and physical properties of OPC, CSA cement, and VCAS pozzolans are presented in Table 1.

Table 1. Chemical compositions and physical properties of OPC, CSA, and VCAS

Properties	OPC (%)	LA – CSA (%)	RH – CSA (%)	VCAS
Silica (SiO_2)	21-22	4.78	7.52	50-55
Alumina (Al_2O_3)	4-6	12.78	27.72	15-20
Iron (Fe_2O_3)	3.2-3.4	0.96	1.44	<1
Calcium (CaO)	63-66	40.40	41.08	20-25
Potassium (K_2O)	0.05-0.1	0.18	0.12	<1
Sodium (Na_2O)	0.05-0.1	0.09	0.10	<0.2
Magnesium (MgO)	1.2	2.77	2.72	<1
Sulfate (SO_3)	2.5-3.5	33.96	14.20	<0.5
Surface area (m^2/kg)	290-390	440	380	-

Note* CS – compressive strength, LA-CSA represented as low alkalinity CSA cement, and RH-CSA represented as rapid hardening CSA cement

2.2 Recycled fine aggregates

RFA used in this study were sourced from crushed concrete with a compressive strength of 50 MPa. The concrete was first crushed into larger pieces and then sieved into two fractions: RFA#1 (with a size of 2.28 mm) and RFA#2 (with a size of 1.07 mm). This process, which involves multiple stages of crushing and sieving, reduces the size of the original recycled concrete aggregates (RCA) into smaller, more usable fine aggregates. These fine aggregates were evaluated for their physical and mechanical properties, as shown in Table 2. The table compares the properties of natural aggregates and two types of RFA (RFA#1 and RFA#2), including maximum size, bulk specific gravity, unit weight, water absorption, moisture content, fineness modulus, and residual mortar. The water absorption and moisture content are higher in the RFA compared to natural aggregates, which impacts the water-cement ratio. To account for this, the water-cement ratio was adjusted to ensure the required mix consistency. Fig. 1a illustrates the different sizes of RFA used, with the yellow arrows pointing out RFA#1 and RFA#2, while Fig. 1b shows the gradation curve for RFA, depicting the particle size distribution. The curve includes upper and lower bound limits, providing insight into the

ideal particle size range for achieving desired concrete properties, and helps determine the suitability of RFA in concrete mix designs. Necessary adjustments have been made to the water-cement ratio to accommodate the higher water absorption of the RFA, ensuring optimal workability and preventing segregation in the mix.

Table 2. Physical and mechanical properties of RFA

Properties	Fine aggregates		
	Natural	RFA#2	RFA#1
Maximum size (mm)	2.36	2.28	1.07
Bulk specific gravity (SSD)	2.68	2.71	2.74
Unit weight (kg/m^3)	1412	1425	1468
Water absorption (%)	1.18	2.28	2.71
Moisture (%)	1.39	2.48	2.61
Fineness modulus	2.65	1.79	1.87
Impact value (%)	-	-	-
Crushing value (%)	-	-	-
Residual mortar (%)	-	30.8	28.8

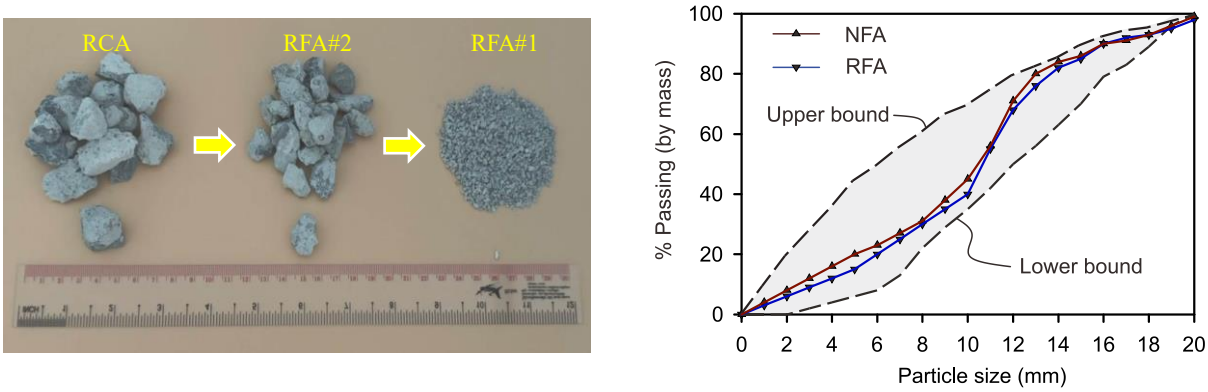

(a) (b)

Fig. 1. Recycled fine aggregates: (a) different sizes of RFA used, and (b) particle size distribution of NFA and RFA.

2.3 Glass fibre reinforcement

In this study, the properties of glass fibre reinforcement were thoroughly evaluated to assess their performance in self-compacting GRC. Key mechanical properties, including tensile strength, elastic modulus, and durability under alkali conditions, were systematically tested to understand the impact of different types of glass fibres on the overall concrete performance. The evaluation focused on the X-2400 (FibreMax-2400 emphasizes high performance) and X-2500 (UltraGlass-2500 emphasizes high strength)

glass fibre types, with attention given to their response to tensile stress, their behaviour in an alkali-rich environment, and their interaction with the CSA cement matrix. These properties are critical for determining the suitability of glass fibres in enhancing the strength, flexibility, and long-term durability of GRC in aggressive environments.

2.3.1 Mechanical characterization of glass fibre: Tensile strength and elastic modulus

In this study, the tensile strength and elastic modulus of glass fibres were evaluated following ASTM D3379-75 (1989) standards [33]. To ensure reliable results, individual filaments from strand bundles were carefully separated, with some fibres experiencing damage during handling, particularly those exposed to alkali conditions. A total of 100 X-2400 and X-2500 types specimens were tested. The testing focused on assessing the mechanical properties of glass fibres, which are critical for their performance in self-compacting concrete with RFA. Due to the fragility of the fibres and their small diameter, the specimens were mounted onto plain paper tabs in accordance with the ASTM guidelines [33]. The filaments were carefully centred over the tab slots and secured using adhesive tape and super glue as shown in Fig. 2a (schematic diagram).

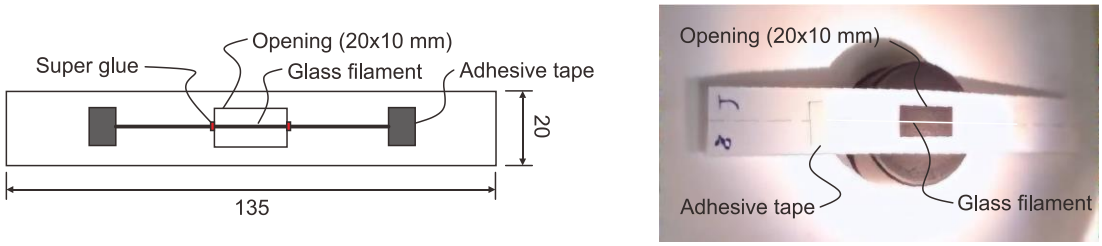

Fig. 2. Single filament of glass fibre: (a) schematic view of the filament, and (b) microscopic examination of the filament (unit in millimetres).

The integrity of each fibre was confirmed under a light microscope to ensure that single fibres were intact (Fig. 2b). Fig. 2b further illustrates the setup of the test specimens mounted and ready for tensile testing. The tensile testing was performed using a universal testing machine, with a load range of 1 N and a crosshead speed of 0.5 mm/min. Each specimen was clamped at the tab ends with precise axial alignment. Tabs were cut at the mid-gauge after clamping to avoid any pre-strain. The test setup and measurement

system used to record load-displacement data during uniaxial tension are shown in Fig. 3a, while Fig. 3b illustrates the load cell and grip used to secure the specimen and measure the applied force.

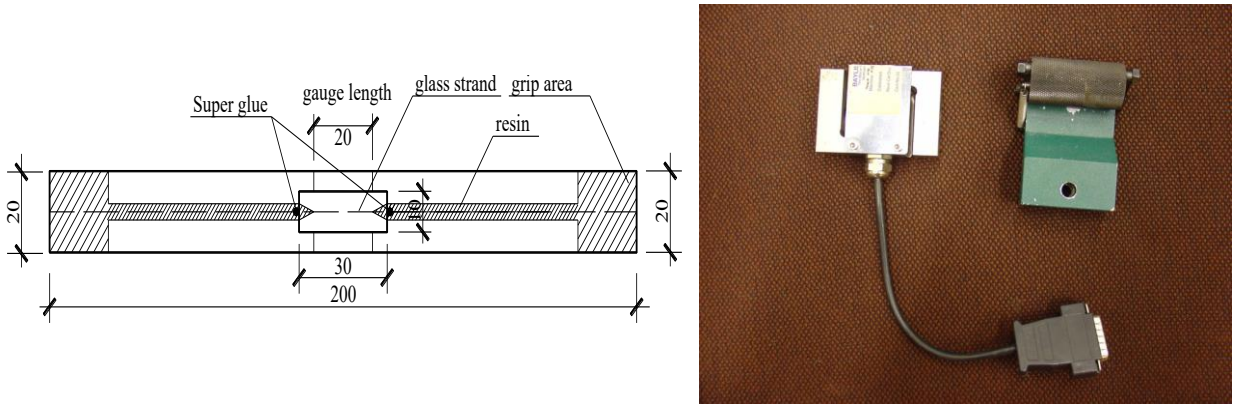

(a) (b)

Fig. 3. Testing preparation of glass fibre: (a) test setup of filament, and (b) load cell and grip (unit in millimetres).

Since traditional methods like strain gauges were not feasible due to the delicate nature of the fibres, an alternative method was employed to calculate the elastic modulus through compliance analysis. The compliance (C) of the fibres was determined based on the load-extension response. This indirect approach avoided the risk of damage to the fibres and provided a reliable measure of the material's stiffness. The compliance data for both X-2400 and X-2500 fibres were plotted as a function of gauge length (10, 20, 30, 40, and 50 mm), as shown in Fig. 4a and Fig. 4b. From these plots, the system compliance (C_s) was calculated, and the true filament compliance (C) was derived by subtracting the system compliance from the indicated compliance. This method proves to be especially effective for evaluating fragile materials like glass fibres, as it minimizes potential damage during testing while still providing accurate strain assessments. The linear regression equations fitted to the compliance data allow for an accurate, non-invasive determination of the tensile strength and elastic modulus of the glass fibres. The compliance data in Fig. 4 shows a clear linear relationship between compliance and filament gauge length for both types of fibres. As the gauge length increases, the compliance also increases, which is expected based on the material’s behaviour under load. The R^2 values of 0.9580 for X-2400 and 0.9874 for X-2500 indicate that the linear model fits the data very well, with more than 95% of the variance in compliance explained by the

gauge length. The higher R^2 value for X-2500 suggests that this fibre type exhibits a more stable and predictable compliance response across different gauge lengths. This strong linear correlation and high R^2 values validate the method as a reliable, non-invasive way to assess the mechanical properties of delicate materials like glass fibres, while minimizing the risk of damage during testing.

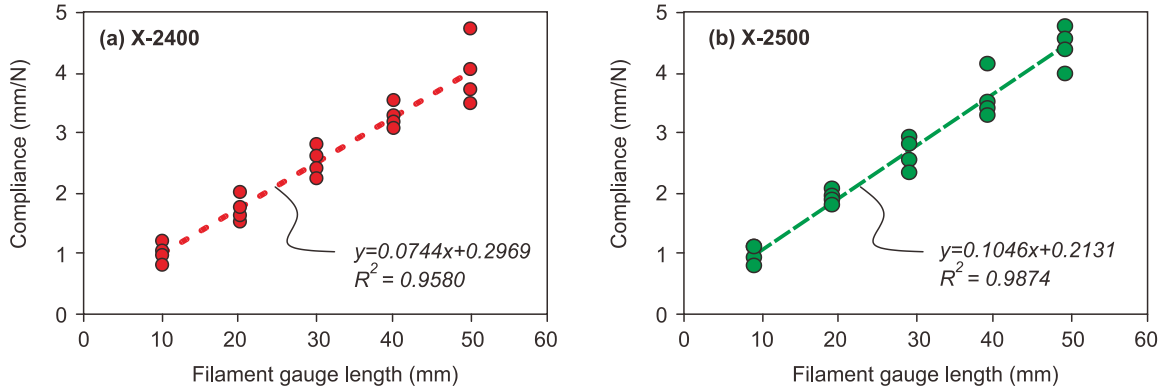

Fig. 4. System compliance for different fibre types based on fibre length: (a) X-2400, and (b) X-2500.

2.3.2 Characterization of glass fibre cross-sectional area

To accurately assess the cross-sectional area of the glass fibres, advanced imaging techniques were utilized, primarily focusing on Scanning Electron Microscopy (SEM). SEM provides high-resolution imaging, allowing for detailed observation of the fibres physical structure at magnifications up to 2500x. This allowed for precise measurement of fibre diameters, which are crucial for determining their mechanical properties and performance in concrete [34]. The process began with the mounting of glass fibres onto sample stubs. As the fibres were non-metallic, they were gold-coated to enhance conductivity for SEM analysis. Fig. 5 presents the SEM photomicrographs of the glass fibres, showing the detailed surface and structure of X-2400 and X-2500 types. The fibres were carefully examined for any inconsistencies or defects that could affect their structural integrity. As shown in Fig. 5a and Fig. 5b, the filament size and the bonding of the fibres are clearly visible, allowing for a thorough inspection of their uniformity. Two distinct methods were employed to measure the cross-sectional area of the glass fibres. The first approach involved determining the area from the mass of a 1-meter strand. This method required careful weighing of the strand, accounting for any sizing content, and then dividing the mass by the known fibre density (2.70 g/cm^3).

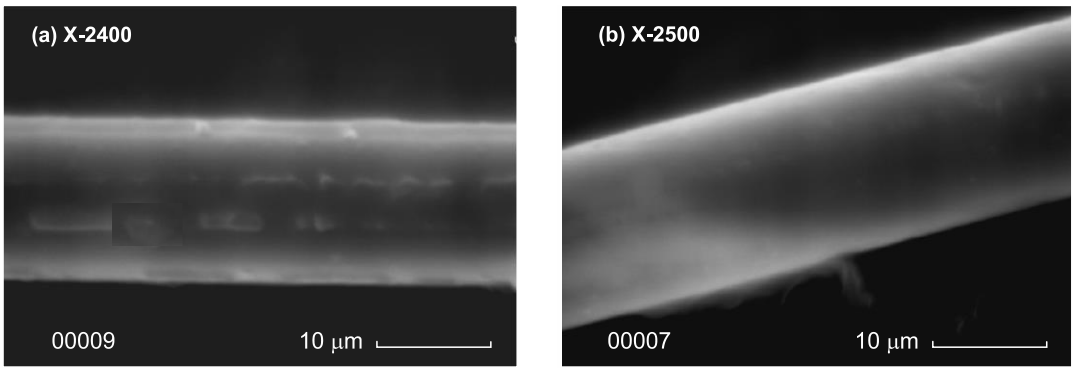

Fig. 5. Photomicrographs of glass fibres (magnification: 2500): (a) X-2400, and (b) X-2500.

This provided an initial estimation of the average cross-sectional area, which was calculated as 0.0326 mm². The second method involved a more hands-on approach using epoxy moulding. Twenty 50mm fibre strands were grouped into two sets and arranged parallel inside a plastic mould. Once the fibres were embedded in liquid epoxy (as shown in Fig. 6a), the epoxy was allowed to harden, forming a solid epoxy coupon (Fig. 6b). After hardening, the coupon was cut and ground, and then gold-coated for SEM imaging. Fig. 6c presents the photomicrograph image of the fibre's cross-section, and the perimeter of the cross-section was extracted using image analysis software to compute the exact cross-sectional area.

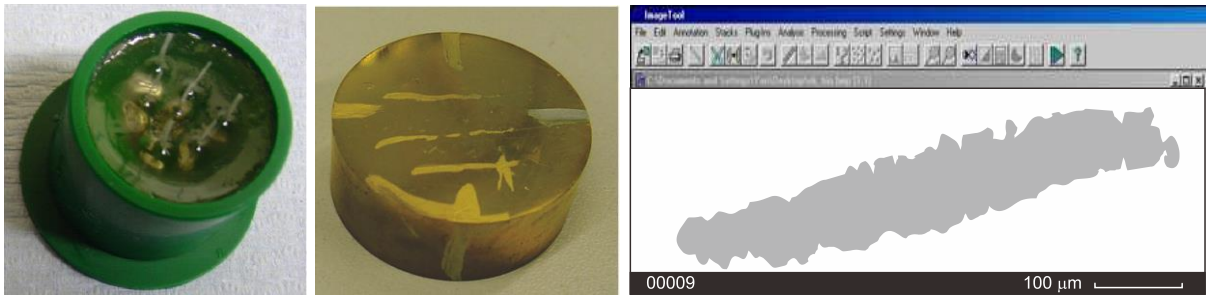

Fig. 6. SEM and photomicrographs tests: (a) mould with epoxy, (b) hardened epoxy, and (c) image analysis of hardened glass fibre.

After analysing the fibre cross-sections using both methods, the average cross-sectional area was determined to be 0.046 mm², calculated through image analysis software. This value was then used in conjunction with the tensile strength data to evaluate the material's strength characteristics. From the experimental tests, the tensile strength of X-2400 was measured in 1738 MPa, slightly lower than the

manufacturer's value of 1800 MPa, likely due to the fragile nature of the fibres. In contrast, X-2500 showed a higher tensile strength of 2652 MPa, outperforming X-2400. The elongation of X-2500 was 3.41%, compared to 2.42% for X-2400, indicating greater flexibility and making X-2400 more suitable for applications requiring higher ductility and resilience. The mechanical properties of two different glass fibres are illustrated in Table 3.

Table 3. Mechanical properties of glass fibres used

Type of Fibers	Length (mm)	Diameter (mm)	Specific gravity	Elastic modulus (GPa)	Tensile strength (MPa)	Elongation (%)
X-2400	10-50	0.02-0.04	2.48	72.3	1738	2.53
X-2500	10-50	0.02-0.04	2.51	78.9	2714	3.38

2.3.3 Durability of glass fibres in alkaline environments

GRC is highly susceptible to degradation when exposed to the alkaline environment within cementitious matrices. To assess the long-term durability of glass fibres, two primary tests were conducted: mass loss and strength retention tests. These tests evaluate the alkali reactivity and performance of the fibres when immersed in a highly alkaline solution. The mass loss test was performed by immersing the glass fibre samples in a saturated calcium hydroxide ($Ca(OH)_2$) solution at a temperature of 80°C for a period of 8 days. This environment simulates the harsh alkaline conditions that the fibres would experience in GRC applications over time [35]. Following the exposure, the samples were dried, and the mass loss was recorded. The results revealed that the X-2400 fibres experienced a mass loss of 2.8%, whereas the X-2500 fibres lost 2.03% of their mass. This indicates that X-2400 fibres exhibit slightly better resistance to alkali-induced degradation, which is crucial for their use in concrete exposed to high pH environments. Table 4 shows the values of mass loss and strength retention tests of glass fibres after exposed to $Ca(OH)_2$. To assess the strength retention of the fibres under alkali exposure, both filaments and fibres were immersed in the same $Ca(OH)_2$ solution. After the exposure period, the tensile strength of the fibres was measured to determine how much strength was retained as shown in Fig. 7. It was found that strand-based fibres exhibited significantly better strength retention compared to individual filaments. Specifically, X-2500 strands retained 82.7% of their initial strength, whereas filaments only retained 30.23% of their original

tensile strength. This suggests that the strand configuration provides better protection against the degrading effects of the alkaline environment, preserving the fibre mechanical integrity over time.

Table 4. Mass loss and tensile strength retention of glass fibres

Fibre type	Before alkali reactivity (g)	After alkali reactivity (g)	Mass loss (%)	pH of saturated $Ca(OH)_2$ solution	Strength retention	
					Filament	Strand
X-2400	2.47	2.40	2.8	12.58	48.83	85.4
X-2500	2.45	2.41	2.0	12.58	30.23	82.7

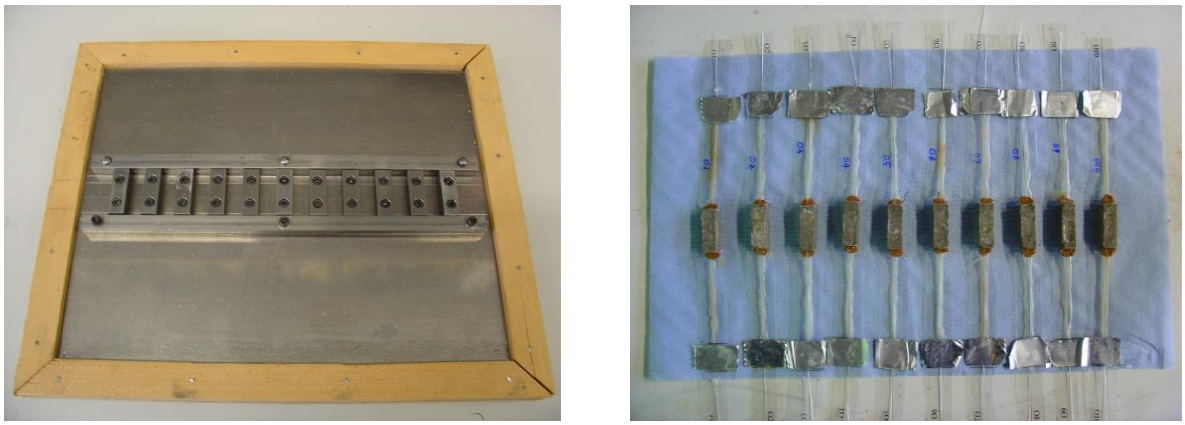

(a) (b)

Fig. 7. Testing preparation of SIC: (a) mould for preparing SIC test, and (b) SIC finished specimens.

2.4 Optimising GRC mixes with recycled fine aggregates

The development and optimisation of GRC mixes involved a systematic investigation into how different variables affect workability, adjusting one factor at a time while considering key interrelationships, such as those between water-cement ratio, RFA, cementitious materials, and superplasticiser content, to determine the optimal values. To evaluate workability, three approaches were employed: Approach 1 utilized the slump test (EN 1170-1, 1998) [36], which measures the spread diameter of the fresh mix to assess the matrix flow; Approach 2 combined the slump test with the flow table test (EN 1015-3, 1999) [37], where vertical jolts simulate dynamic conditions, capturing the thixotropic behaviour of the GRC, suited for low to moderate workability mixes; Approach 3 used a flow funnel test, adapted from the V-Funnel test (EFNARC, 2001) [38], to measure the flow time through a 20 mm spout, evaluating viscosity, filling ability, and segregation resistance in highly flowable mixes. These complementary approaches provided a comprehensive assessment of different GRC consistencies and their suitability for practical application

scenarios as shown in Fig. 8.

(a) (b) (c)

Fig. 8. Workability test approaches: (a) slump test as per EN 1170 [36] (b) flow table combined with EN 1170 with EN 1015 [36, 37], and (c) V-funnel test [38].

To determine the optimal mix design, nine formulations containing CSA cement, OPC, PFA, and GGBS were tested for workability using Approaches 1 and 2, with RFA and water kept constant at 70 kg/m³ and 40 kg/m³, respectively. The results showed similar workability in GRC mixes made with OPC and CSA cement, while OPC-CSA blends slightly reduced the workability. The detailed formulations and results of different mixes with glass fibres are provided in Table 5. Replacing PFA in the mixes led to a small improvement in workability compared to GGBS [39]. The effect of mix designs on workability was also examined using RFA, which highlighted the role of different cementitious materials and their interactions in optimizing the workability of the mixes is illustrated in Appendix A.1. Additionally, white Portland cement (WPC) mixes were evaluated and the mix the details using RFA is shown in Appendix A.2. Although WPC mixes, chemically like OPC, initially exhibited poor workability, the addition of superplasticiser and SPFA significantly improved the workability.

Table 5. Mix details of OPC and CSA cement on workability

Mix	OPC	CSA	PFA	GGBS	Fibre (%)	Workability approaches (mm)		
						1 (mm)	2 (mm)	3 (Sec)
1	100	-	-	-	3	95	150	10
2	-	100	-	-	3	90	150	11
3	80	20	-	-	3	95	150	10
4	50	50	-	-	3	65	135	12
5	-	70	30	-	3	95	160	14
6	-	60	40	-	3	85	140	16
7	-	50	50	-	3	90	165	15
8	-	70	-	30	3	80	145	18
9	-	50	-	50	3	75	145	20

When WPC is combined with glass fibres, there is typically a decrease in workability due to the increased viscosity and resistance to flow caused by the fibres with the addition of RFA. To counteract this reduction, the addition of superplasticisers and supplementary materials such as SPFA is necessary. These additives help improve the fluidity of the mix, ensuring even dispersion of the fibres throughout the concrete. As a result, the workability is enhanced, maintaining the required consistency for proper application and ensuring the quality of the final GRC product.

2.4.1 Optimisation of GRC mixes with SCC and RFA

The development and optimization of GRC mixes were carried out to identify the best mix design that ensures high workability and consistent performance. The study focused on adjusting the key parameters such as the water-cement ratio, cementitious material content, and the incorporation of RFA, along with the addition of fibres and superplasticizers to enhance fluidity and dispersion. The superplasticizer dosage was optimized through a series of trials, ranging from 0.5% to 1.5%, and was determined based on the results of the flow time tests and visual assessment of the cylinder surfaces. The optimal dosage was found to be around 1%, as it provided the best balance of plasticizing effectiveness without increasing cost. Both X-2400 and X-2500 fibres were used in all tests, and their impact on workability was assessed by measuring the flow speed of the slurry before and after adding fibres. The mix design and flow time have been measured for various trails and errors to optimise the fibre as well as RFA through different approaches and different fibres are tabulated in Appendix A.3. Fig. 9 shows the workability of approaches 1 and 2 with the glass fibre content. The mix design was formulated with a constant ratio of 1-part OPC and 1 part CSA cement, along with 1-part RFA. The water-cement ratio was kept constant, and a superplasticiser dosage of 0.3 and 1% were applied to all mixes to evaluate the flow properties of SCC [39]. From Appendix A.3, the flow performance of SCC with RFA and GRC shows that increasing fibre content typically reduces flowability due to higher internal friction. High-strength fibres like X-1000 maintain better flowability at higher dosages compared to fine fibres such as UF-300, which significantly hinder flow. The addition of superplasticizers improves flow by dispersing fibres and reducing the viscosity, particularly in mixes with

higher fibre contents as shown in Fig. 9a. A lower water-cement ratio (0.32–0.36) further enhances flow characteristics while balancing strength. Overall, the results suggest that optimizing fibre type, content, and water-cement ratio, along with superplasticizers, is crucial for achieving the desired flowability and performance in sustainable GRC mixes.

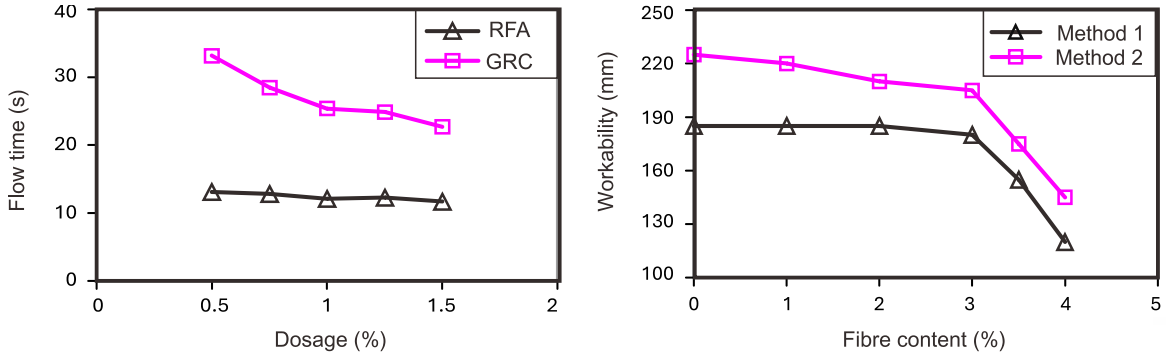

Fig. 9. Optimisation of fibre content: (a) flow time vs fibre content, and (b) effect of workability with fibre content.

The impact of fibres on workability was significant. Higher fibre contents increased the resistance to flow, which is a typical characteristic of GRC due to the fibres creating more internal friction as shown in Fig. 9b. Additionally, fibre type, size, and strand configuration were key factors influencing the workability of the mix. Medium-integrity fibres (such as those typically used in specialist premixes) showed a significant reduction in flowability during mixing, whereas high-integrity fibres provided better results in terms of flowability. To improve the flowability of high-fibre content mixes, polymer emulsions were added at 10% by cement weight, which reduced the water-cement ratio to 0.32. The addition of superplasticizers and SPFA also helped enhance the fluidity and workability of the mixes. Further adjustments were made with the addition of antifoaming agents to reduce air content and improve flowability.

2.5 Evaluation methods for mechanical properties of GRC

This section outlines the test methods used to assess the mechanical properties of GRC, including compressive strength to evaluate load bearing capacity, double-sided pull-out tests for fibre-matrix bond strength, and bending tests to determine flexural behaviour. These tests provide a comprehensive evaluation

of GRC with CSA and RFA performance under various loading conditions.

2.5.1 Compressive strength

Compressive strength tests were performed on 50 mm cubic specimens using a standard compression testing machine, following the EN 12390-3 (2002) standards [40]. The specimens, incorporating RFA as a complete replacement for natural fine aggregates, were subjected to curing at different temperatures (20°C, 38°C, and 60°C) to assess their impact on early and long-term strength development. The influence of RFA on compressive strength was compared to control mixtures using OPC and CSA cement. Additionally, the effect of glass fibre reinforcement on compressive strength was evaluated for each mix, and specimens were tested. The compressive strength was calculated from the maximum load at failure, with three specimens tested per condition to ensure accuracy.

2.5.2 Bending test of CSA-GRC with recycled aggregates

Bending tests were conducted on SC-GRC specimens made with 100% RFA to evaluate their flexural performance and compare it with conventional concrete mixes. Extensive tests were conducted to assess the impact of various factors on flexural behaviour, including fibre type, fibre content, curing conditions, binder type, modifiers, and casting techniques. The findings contributed to the development of mechanical models for analysis and design. The specimens were fabricated using consistent materials and manufacturing processes, ensuring that the inclusion of RFA did not alter the general procedure. Small batches were cast using an acrylic mould with three timber sides and two acrylic face plates, secured with screws, while larger batches utilized a 600 × 600 mm polyurethane rubber mould as shown in Fig. 10a to facilitate easier demoulding and improve durability. A custom designed testing rig was employed to apply load while measuring the deflection response at small load scales. Load was applied manually by rotating a handle, with a 1.50 kN load cell used to measure the applied force. The deflection at mid-span and at the bottom support area was recorded using Linear Variable Differential Transformers (LVDTs) as shown in Fig. 10b. The data were logged using an ORION data logger and transferred to a desktop PC for continuous monitoring and analysis. Each full rotation of the loading bolt produced a vertical displacement of 1.50

mm, with the load application rate set at 0.03 mm/s displacement, in accordance with EN 1170-5 (1997) [41]. This allowed a full rotation to occur approximately every 20 seconds, enabling accurate measurement of the bending response of the SC-GRC mixtures containing RFA at varying replacement levels. A variety of mix designs were developed with different fibre types and amounts, using a constant 1:1 ratio of OPC or CSA cement to RFA. These mixes included various formulations with different dosages of Flowaid SCC and fibres, such as 13PH901X, 350Y, and 530X, along with additional modifiers. The objective was to assess the impact of RFA and fibre content on the workability, strength, and durability of the concrete, while maintaining the 1:1 cement-to-RFA ratio, ensuring consistency across all trials.

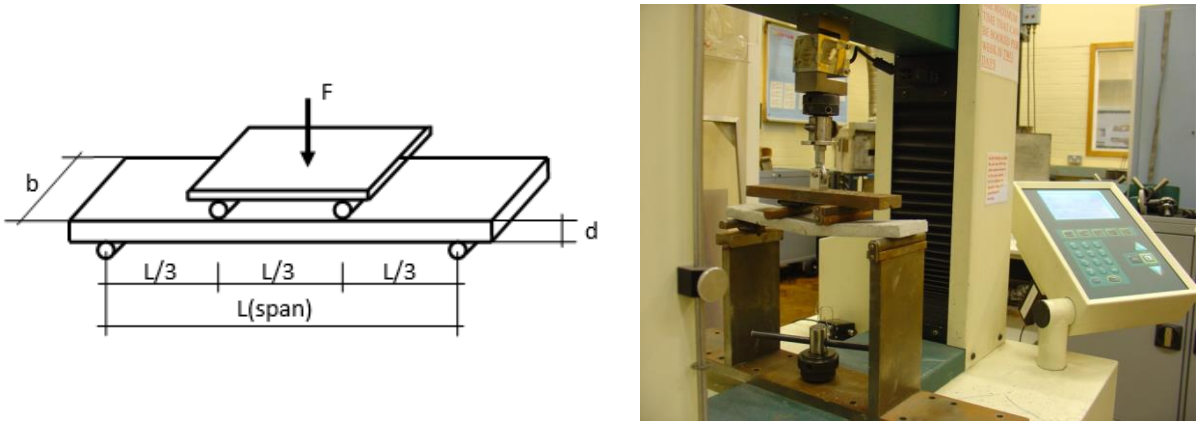

(a) (b)

Fig. 10. Bending test: (a) bending strength test specimen, and (b) test setup of bending test.

2.5.3 Bond strength evaluation using double-side pull-out test

The double-side pull-out test was used to assess the bond strength between the glass fibre strands and the concrete matrix, minimizing variability in results. In this test, three 200-filament strands were embedded in either OPC or CSA cement matrices, with a polystyrene block placed between them to simulate the presence of a crack. Specimens were subjected to uniaxial tension at a constant displacement rate, with all strands having equal embedment lengths to ensure uniform load sharing. A mould made from plywood and chipboard produced 20 pull-out specimens, each cast in two 60 × 60 × 20 mm blocks, separated by a 15 mm polystyrene block wrapped in polytetrafluoroethylene to prevent bonding as shown in Fig. 11a. Three 2-mm plastic tubes were used to allow fibres to pass through, and plasticine was applied to the initial fibre

length to control the bond length and minimize surface cracking. The tests were conducted using a universal testing machine with a 1 kN load cell, and displacement was controlled at a rate of 0.5 mm/min. Load and displacement data were recorded digitally and displayed in real time on a PC connected to the testing machine, as shown in Fig. 11b. The bond strength (τ) is determined by dividing the maximum load (P) achieved by the product of the number of fibre strands (n), the strand perimeter at the interface (p), and the embedment length (l). This formula provides a measure of the adhesion between the fibre strands and the cementitious matrix.

(a) (b)

Fig. 11. Double side pull-out test: (a) pull-out test specimen, and (b) test setup of pull-out test.

2.5.4 Time dependent long-term properties

The strength and ductility of GRC tend to decrease over time, particularly when exposed to hot, damp, or wet environments. Both the modulus of rupture (MOR) and strain to failure gradually decline to a stable level, with the MOR approaching the long-term limit of proportionality (LOP), which may slightly increase due to ongoing cement hydration. To ensure safety, strength degradation must be accounted for in design. Strategies to improve GRC aging performance generally involve altering glass fibre composition or surface treatment or modifying the matrix. Three 1.2 × 1.2 m GRC boards were produced using the hand-spray method, incorporating various materials, including VCAS pozzolan and acrylic polymer emulsion, to assess their impact on long-term properties. After 28 days of curing, the boards were cut into 64 standard test coupons (EN 1170-5) [41], with 8 serving as controls and 56 immersed in water baths at 60°C for aging. Bending tests were conducted at various intervals of aging. A separate 1 m × 1 m test board, cast using

premixed GRC with 2.5% chopped strands and a 0.32 water-cement ratio, was also produced. Different glass fibre meshes were applied in one or two layers, with an unreinforced GRC panel serving as the control. After 28 days, this board was cut into coupons specimens and were immersed in a 60°C water bath for further testing as shown in Fig. 12.

(a) (b)

Fig. 12. Long-term test: (a) coupon specimens for test, and (b) specimens at 60^{o} C in water bath.

3. Results and discussion

This section presents and analyses the key findings of the study, focusing on the mechanical properties, strength results from experimental tests, and the durability performance of GRC elements incorporating RFA. The discussion highlights the implications of these results for the structural behaviour and long-term performance of GRC elements, particularly with the inclusion of CSA and recycled fine aggregates.

3.1 Strength development of mortar in CSA and RFA

The compressive strength of mortar incorporating CSA and OPC was evaluated at different curing temperatures, with the results depicted in Fig. 13. In Fig. 13a, the compressive strength results at different temperatures (20°C, 38°C, and 60°C) show that CSA outperforms OPC when exposed to high curing temperatures. At 38°C, CSA maintained a strength of 47 MPa, while OPC dropped to 38 MPa. At 60°C, CSA showed a reduction to 41 MPa, while OPC experienced a larger decline to 34 MPa. This indicates that CSA retains a significantly higher strength than OPC at elevated temperatures, with CSA showing only a 2-3 MPa reduction at 60°C. These results attribute that CSA maintains its strength better under high curing temperatures, likely due to its faster early-age hydration and reduced sensitivity to temperature variations, in contrast to OPC, which is more vulnerable to thermal degradation [42].

The compressive strength at later curing ages (17, 34, and 51 days) further confirms the stability of CSA as shown in Fig. 13b. At 17 days, CSA reached a strength of 49 MPa, while OPC had a strength of 46 MPa. By 51 days, CSA had achieved a strength of 55 MPa, whereas OPC increased to only 52 MPa. The results demonstrate that CSA maintains a more stable and consistent strength profile over time compared to OPC, which shows slower strength development [43]. These findings reveal that CSA has superior long-term stability under high temperature curing conditions, making it a promising alternative for applications in hot climates or during rapid concrete production processes. The inclusion of RFA did not significantly affect the compressive strength. For instance, CSA with RFA at 28 days showed a strength of 55 MPa, compared to CSA without RFA, which showed a strength of 56 MPa. This indicates that RFA can be effectively used as a sustainable substitute for natural aggregates in CSA mixtures without compromising the compressive strength, supporting previous studies that suggest RFA can yield comparable or even improved results when used with alternative binders like CSA.

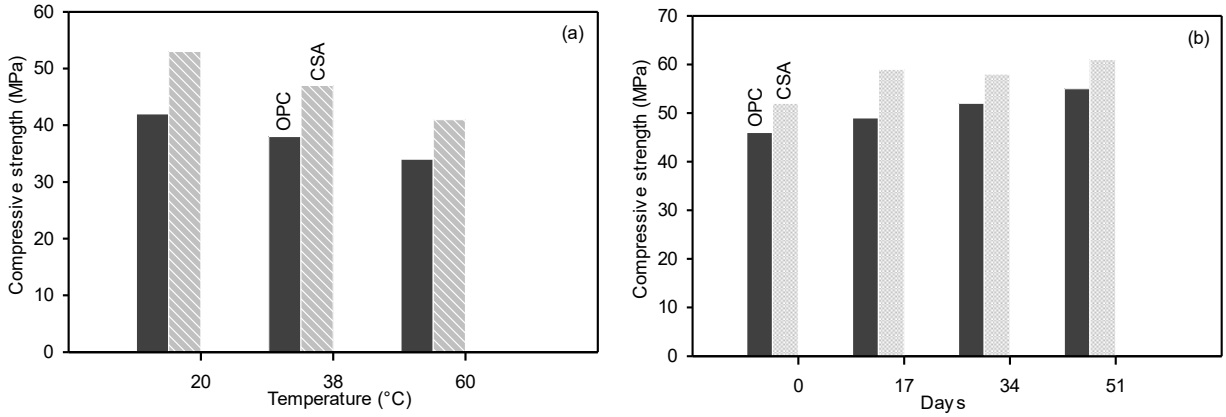

Fig. 13. Compressive strength: (a) effect of initial curing temperature on strength, and (b) effect of high curing temperature (60°C) on strength development of mortar.

3.1.1 Comparison of OPC, CSA, and their blends with RFA in GRC

In this study, OPC, CSA cement, and OPC/CSA blends (2:1 ratio) were tested for compressive strength after 28 days of curing at 20°C and 100% relative humidity. The OPC/CSA blend cubes showed a rougher surface finish with defects, and upon failure, the upper part disintegrated into crumbs, as shown in Fig. 14,

unlike the typical cone-shaped fracture of CSA. The CSA+RFA sample, shown in the bottom left of the photo, exhibited a more intact structure upon failure, with minimal surface cracking, highlighting the potential of combining CSA and recycled fine aggregate for enhanced durability. The primary variable was fibre content, ranging from 0% to 4%, and the effect of recycled fine aggregate replacing sand was also evaluated. The mix designs and corresponding 28-day compressive strength results are shown in Appendix B.1.

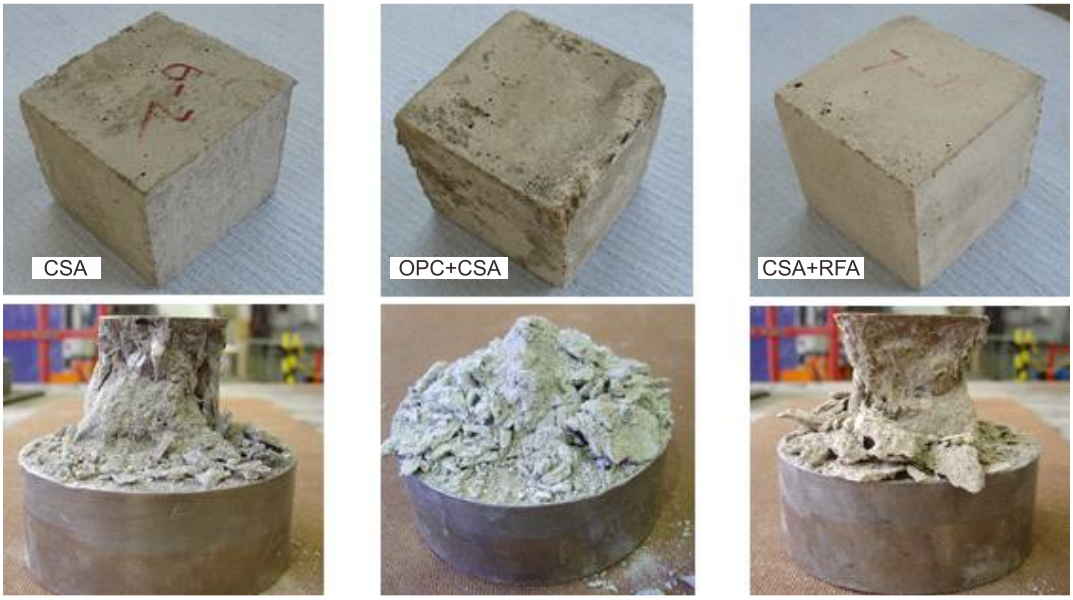

Fig. 14. Compressive strength failure of specimens before and after testing.

The results presented in Appendix B.1 show that increasing fibre content slightly reduced the compressive strength of GRC, with an approximate decrease of 0.8 MPa per 1% increase in fibre content. This suggests that, under compression, the fibres behave similarly to voids. As shown in Fig. 15a, the compressive strength results of CSA, OPC, and their blends with RFA were consistent over time. At 28 days, CSA with RFA achieved a compressive strength of approximately 55 MPa, while CSA without RFA reached 56 MPa. This indicates that RFA has minimal impact on the compressive strength, supporting its use as a sustainable alternative to natural sand without compromising the material performance. In Fig. 15b, the compressive strength results in relation to fibre content show that increasing fibre content does not significantly improve the compressive strength but does enhance the strain capacity and post-cracking toughness of the concrete.

At fibre contents between 1% and 3%, CSA+RFA exhibited stable strength, with a slight decrease in compressive strength as fibre content increased. This suggests that the fibres contribute to improving the toughness and ductility of the material, rather than significantly enhancing its compressive strength.

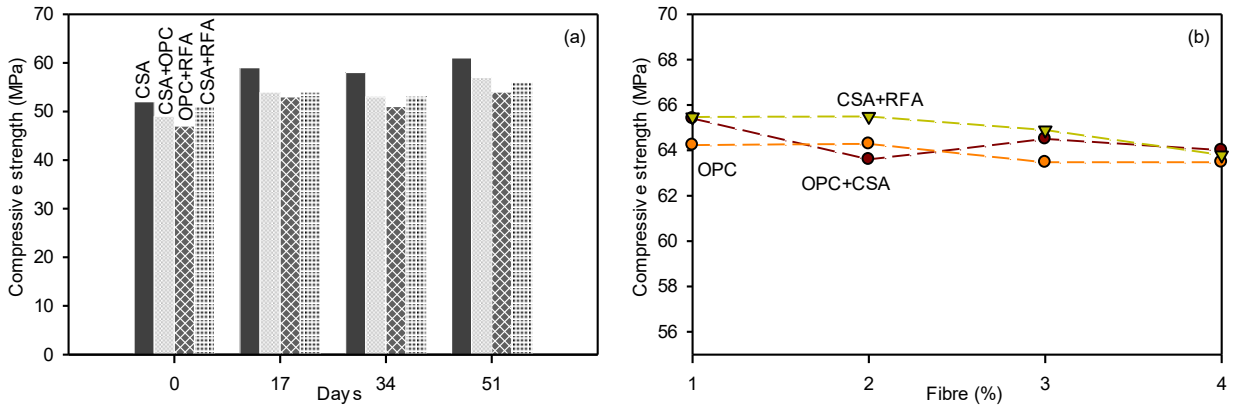

Fig. 15. Compressive strength: (a) strength development of OPC, CSA with RFA over time, and (b) effect of fibre content on strength development.

3.2 Flexural performance of GRC with RFA

Extensive tests were performed to evaluate the flexural behaviour of GRC under different parameters. Variables included fibre type and dosage, curing conditions, binder composition with RFA, use of modifiers, and casting techniques. The designed mix data is shown in Appendix A.1 to A.3. Fibre contents ranged from 2 to 4%, while curing was done at 20 °C and 60 °C for various durations. Binders such as OPC, CSA, and their blends with RFA were examined, along with modifiers like superplasticiser, acrylic polymer, and antifoaming agent. All the specimens were tested under a Hounsfield universal test machine as discussed in test methods section to get a typical load-deflection curve obtained from data acquisition system as shown in Fig. 16a. A customized third point bending rig, shown in Fig. 10b, was developed to perform flexural tests in accordance with EN 1170-5 [41] standards. Data from identical mix specimens were processed using Compaq Visual FORTRAN 6.6 to obtain averaged values. Typical load deflection curves and the averaged results are presented as shown in Fig. 16b, while the complete dataset is provided in Appendix C.1. These results were used to determine the flexural modulus of elasticity (E), limit of proportionality (LOP), and modulus of rupture (MOR), forming the basis for evaluating the flexural performance of the tested mixes.

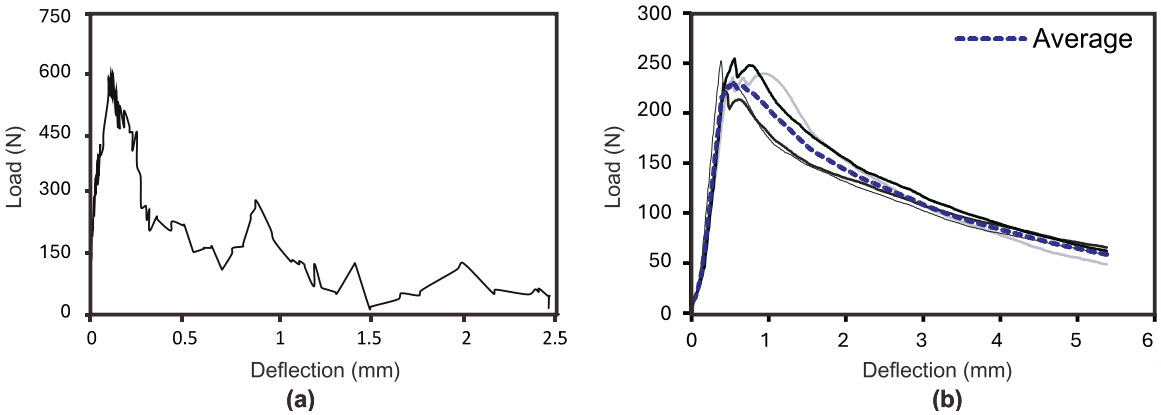

Fig. 16. Flexural strength: (a) typical load deflection response, and (b) average load deflection response.

3.2.1 Modulus of elasticity and limit of proportionality

The flexural modulus of elasticity is defined as the ratio of stress to strain within the elastic limit of a material. In the case of a third point bending test, E is determined from the load-deflection data, as shown in Appendix C (Fig. C.2). To account for fluctuations in the load-deflection curve, a smoothing technique was applied to reduce noise and enhance the accuracy of the modulus calculation. Typically, E is calculated by measuring the slope between successive load steps. To improve precision, a weighted average of the adjacent five points was used, with the resulting value representing a more reliable estimate of the flexural modulus. This method ensures a more stable and representative modulus by minimizing the effects of data irregularities. The smoothing process was repeated several times, and after four iterations of averaging, the curve stabilized, with no significant changes observed in subsequent rounds. The maximum value of the flexural modulus, referred to as E_{max}, was extracted from the smoothed graph. This value represents the final flexural modulus of elasticity, providing a consistent measure of the material's stiffness under bending.

The LOP represents the stress point at which the stress-strain curve deviates from linear elasticity, signalling the onset of non-elastic behaviour. Identifying this point experimentally is challenging and often subjective. In this study, two methods were used to determine the LOP: statistical analysis and trendline fitting. Initially, the LOP was manually selected from the load-deflection data for each specimen, and the corresponding elastic modulus (E_{LOP}) was calculated. Theoretically, E_{LOP} should be equal to the maximum flexural modulus (E_{max}), with a noticeable decrease in E following the LOP. The ratio of E_{LOP}/E_{max} was computed,

revealing significant scatter in the results. To refine this, statistical analysis was conducted using the MINITAB software, generating histograms and probability distribution curves, as shown in the Appendix C. The 3-parameter Weibull and Smallest Extreme Value distributions were found to best fit the data, as seen in Appendix C.3. These distributions are commonly used in engineering to model failure times and describe the delay in reaching the LOP. The Anderson-Darling statistic for both distributions was nearly identical (1.596 and 1.593), as shown in the probability plot Appendix C.4. This statistical approach models the minimum values from a large set of observations, typically skewed to the left, with most data points clustering at the upper tail. For E_{LOP}/E_{max}, values mainly ranged between 0.65 and 0.95, with a few below 0.45. Since the E_{LOP}/E_{max} values did not follow a normal distribution, the highest probability value, 0.82, was chosen to calculate the LOP.

After reaching Emax, the ratio E_{LOP}/E_{max} was plotted against the normalized equivalent flexural strength ratio σ/LOP, as shown in Fig. 17. For simplicity, σ was calculated until the elastic modulus, E, decreased to half of its maximum value. A 4th-order polynomial trendline was fitted to the data. The intersection of this trendline with the line σ/LOP = 1 gives an E/E_{max} value of 0.85, which serves as the objective criterion to determine the LOP point. The previously estimated E_{LOP}/E_{max} value from statistical analysis was 0.82, which is close to 0.85, but using the lower value would result in a higher LOP stress. To adopt a more conservative approach, the 0.85 value was selected to define the LOP.

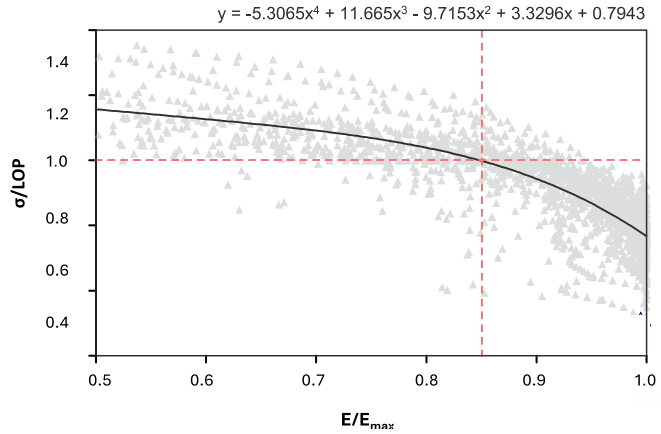

Fig. 17. *σ*/LOP versus *E/E*$_{max}$ chart

3.3 Influence of CSA with RFA and GRC on flexural strength and curing temperature

As shown in Fig. 18a, the inclusion of RFA in CSA-based GRC improved flexural performance. CSA–RFA achieved a modulus of elasticity of 17 GPa, slightly higher than CSA's 15 GPa, due to a denser microstructure that enhances the bond between the matrix and fibres. In contrast, CSA–OPC blends showed a 10% lower MOR, likely due to incompatibilities between the two binders, as shown in Fig. 18b. Compared to OPC-based mixes, CSA–RFA exhibited higher stiffness, with an elastic modulus of 17.5 GPa, while OPC-based mixes reached 15 GPa. This improvement is attributed to CSA's expansive hydration products, which reduce microcracking around RFA particles and enhance matrix continuity, compensating for RFA's higher porosity.

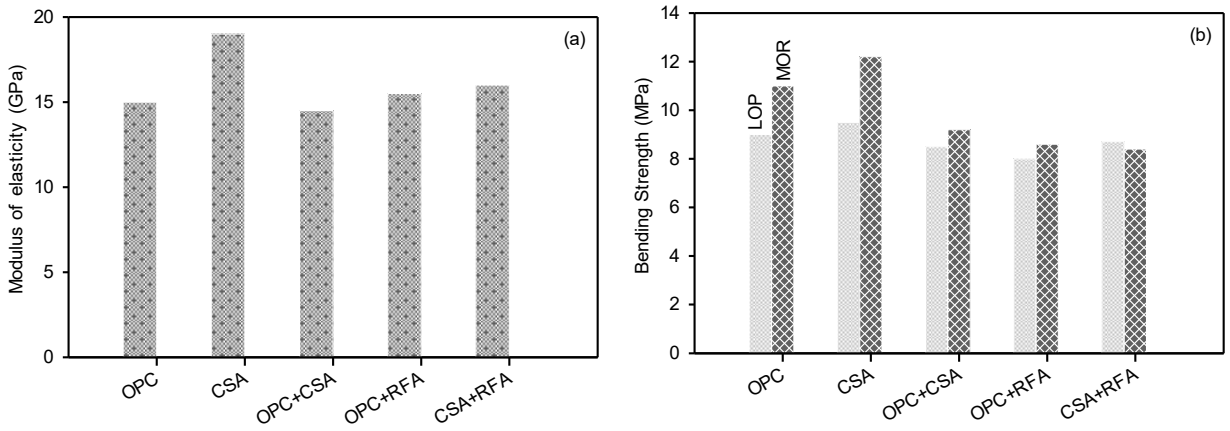

Fig. 18. Bending strength: (a) effect of cementitious materials on bending strength, and (b) effect of bending strength (MOE and LOP).

The effect of curing temperature and duration on the flexural performance of CSA–RFA is presented in Fig. 19. During the early curing period (up to 17 days), both the elastic modulus and flexural strength remained relatively stable across temperatures up to 60°C, showing robust early-age performance. As shown in Fig. 19b, CSA–RFA mixes retained an elastic modulus of around 16 GPa at 60°C after 17 days, like the control. However, with prolonged exposure beyond 34 days, a gradual reduction in both parameters was observed, with elastic modulus dropping by about 2 GPa at 51 days. This reduction is not attributed to matrix degradation but rather to the progressive deterioration of fibre-matrix interfaces under sustained heat, leading to minor reductions in post-cracking resistance.

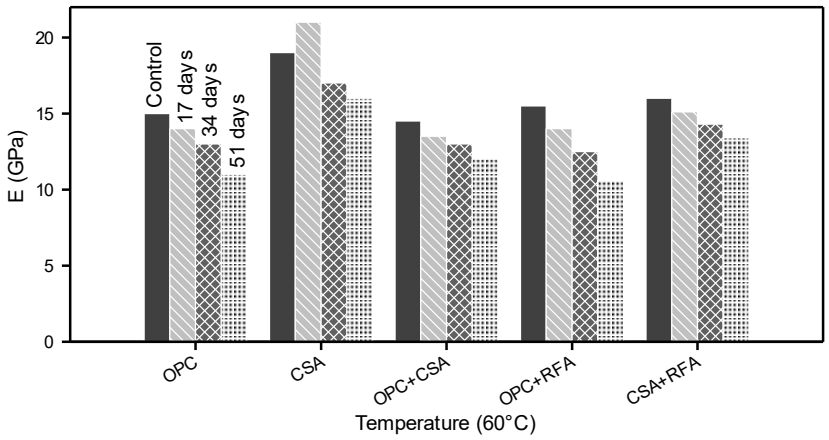

Fig. 19. Effect of curing temperature (60°C) and time on MOE of OPC, CSA and RFA.

Despite this, the CSA–RFA composites retained a higher percentage (around 90%) of their initial flexural capacity compared to conventional mixes, which exhibited a 10-15% decrease. This demonstrates superior thermal stability, as CSA-based mixes can maintain performance under higher temperatures for extended periods. Microstructural observations revealed that the ettringite-rich matrix in CSA cement provided self-healing potential under moist high-temperature conditions, reducing crack propagation over time. These results highlight the suitability of CSA–RFA for applications in hot and humid climates, where conventional GRC tends to lose ductility more rapidly.

3.4 Pull-out test with double sided bonding

The bond strength results of CSA specimens with RFA in GRC are presented in Appendix D.1. The test regimes, represented by groups 1 to 8, were conducted with various fibre lengths, ageing temperatures, and ageing times. For example, group 6 represents CSA specimens with 8 mm fibre length, aged at 38°C and 100% relative humidity (RH) for 14 days. As seen in the table, the peak load for CSA specimens with RFA ranged from 15.0 N to 38.0 N, with corresponding average bond strengths between 0.50 MPa and 0.62 MPa. The average tensile strength for OPC was 41.5 MPa (σ = 1.7 MPa) and for CSA was 39.3 MPa (σ = 1.6 MPa), indicating a slight reduction in tensile strength for CSA compared to OPC. However, RFA inclusion did not have a significant impact on the tensile strength or the bond strength between the fibre and matrix. The peak load for CSA with RFA ranged from 14.7 N to 26.3 N, and the average bond strength

ranged from 0.50 MPa to 0.61 MPa. This suggests that while RFA slightly reduced the compressive strength, it did not negatively impact the pull-out test performance or the fibre-matrix bond strength, which governs the mechanical behaviour. All specimens failed by strand pull-out, with the maximum tensile stress ranging from 84.9 MPa to 387.5 MPa, far lower than the tensile strength of the fibres (1602 MPa). These results confirm that the bond strength between the fibres and the matrix is the primary factor influencing the mechanical performance of GRC, rather than the intrinsic tensile strength of the fibres themselves. The inclusion of RFA did not significantly alter the fibre-matrix bond, supporting RFA use as a sustainable alternative in GRC.

3.4.1 Influence of fibre matrix bonds, fibre length and ageing temperature

The embedment length significantly influences the pull-out behavior, offering valuable insights for optimizing fibre length. As shown in Fig. 20, bond strength increases with embedment length, peaking at 8 mm before slightly declining. At 10 mm, strand pull-out occurred from the anchorage side, suggesting that the optimal embedment length is around 8 mm, which corresponds to an ideal fibre length of approximately 16 mm. In practice, fibres are often chopped to 25 mm. The embedment length is influenced by fibre integrity, bonding capacity, and matrix characteristics. In RFA-incorporated GRC, the angular shape of RFA improves mechanical interlocking with the matrix, enhancing bond strength compared to traditional sand matrices. The presence of RFA did not significantly reduce bond strength, confirming its suitability as a sustainable alternative without compromising performance.

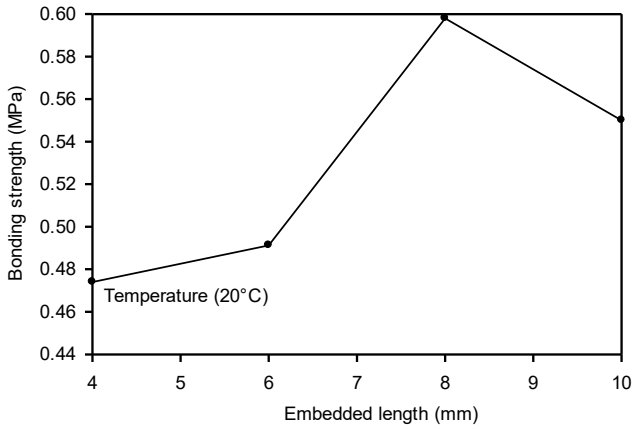

Fig. 20. Relationship of bond strength and embedded length.

Fig. 21a presents the bond strength of OPC specimens with 6 mm fibre embedment increases with ageing time, reaching a peak at around 60 days. This initial increase is attributed to the strengthening of the matrix as hydration progresses. After this peak, bond strength begins to decline due to chemical degradation at the fibre-matrix interface, which weakens the bond over time. Fig. 21b further demonstrates that with extended ageing time, bond strength progressively decreases, reflecting the long-term effects of degradation at the interface. This trend is consistent for both OPC and CSA-based mixes, showing that the bond strength is sensitive to prolonged ageing. The bond slip behaviour of pull-out specimens of CSA with RFA and GRC is illustrated in Appendix D.2. The inclusion of RFA slightly improves bond strength compared to the traditional sand matrix, as RFA's angular particles enhance mechanical interlocking with the matrix, which contributes to better load transfer. However, the degradation trend at longer ageing times is still evident in the RFA-incorporated mixes, like the standard mixes. This suggests that while RFA improves the mechanical bond, it does not significantly alter the overall degradation pattern due to ageing. These results indicate that both ageing time and the fibre-matrix bond are crucial factors in determining the long-term performance of GRC. Managing the ageing process is key to maintaining optimal bond strength, and while RFA provides slight improvements, it does not completely mitigate the effects of ageing. The use of RFA remains beneficial in providing a more sustainable alternative without drastically compromising performance.

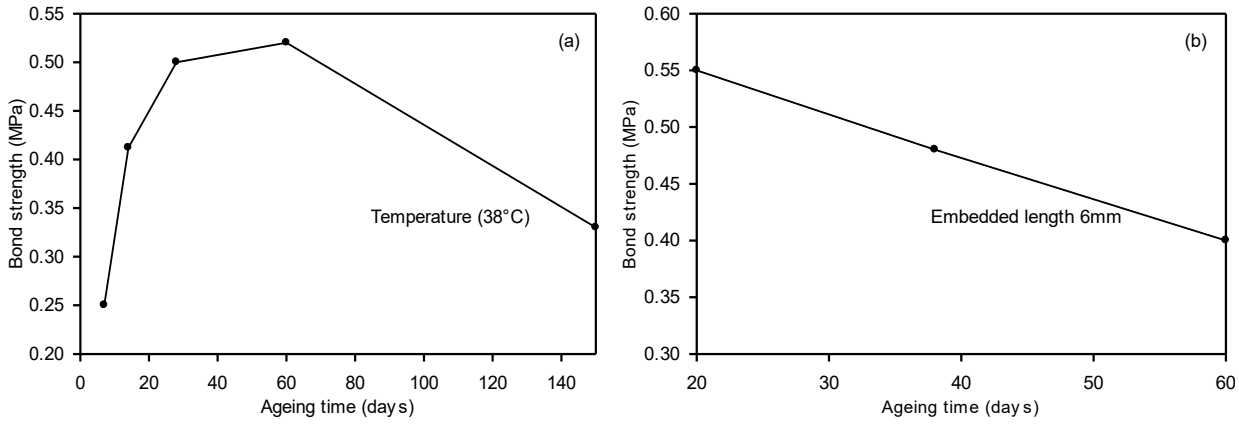

Fig. 21. Effect of ageing on bond strength: (a) bond strength over varying ageing times at 38°C, and (b) bond strength of 6 mm embedment fibre over different ageing durations.

3.5 Long-term performance

The elastic modulus of OPC-based GRC specimens stored in water for three years was approximately 30% higher than that of specimens cured under standard conditions, with flexural strength increasing by about 5%. These results indicate that cement hydration continues beyond the typical 28-day curing period, contributing to enhanced mechanical properties over time. In the case of RFA incorporation, similar trends were observed, with RFA contributing to enhanced mechanical properties. The RFA mix showed a modest increase in elastic modulus and flexural strength, consistent with better fibre-matrix bonding, as shown in Appendix D. These results confirm that cement hydration continues well beyond the standard curing period, and the long-term mechanical properties of GRC can be further enhanced by incorporating RFA, particularly in terms of fibre-matrix interaction. However, it is important to note that over time, the cement matrix can degrade due to environmental exposure, which may lead to a gradual decline in the overall properties of the composite. Despite this, RFA remains a viable and sustainable alternative that enhances mechanical properties and bonding, making it a good option for GRC applications.

3.5.1 Effect of fibre content with CSA-RFA

The influence of fibre parameters, including content, length, and type, on the elastic modulus is shown in Appendix E.2. The results indicate that in the fibre content range of 2% to 4%, there is little change in the elastic modulus, which varies between 14 GPa and 18 GPa. This suggests that the fibre content in this range has minimal impact on the modulus, although the modulus of AR glass fibres is significantly higher than that of mortar and RFA. As Appendix E.3 shows, the LOP and MOR increase with higher fibre content, but for fibres with low integrity or poor strand configuration (e.g., NSH and 350Y), a reduction in strength is observed. This could be due to the higher fibre content impairing the workability of the mix, leading to a less dense GRC matrix. Furthermore, higher fibre content may result in increased fibre entanglement, which can reduce the overall effectiveness of the fibres in reinforcing the matrix, especially in mixes with poor fibre integrity.

3.5.2 Time dependent properties

Three matrices were considered to study the time-dependent performance: Matrix A (with OPC + GRC), Matrix B (with CSA + GRC), and Matrix C (with CSA + RFA + GRC). The time required for MOR and STF to decrease by half was significantly influenced by the type of matrix used. As the results shown in Appendix E.1 and E.4, matrix "A" showed a more rapid decline in both MOR and STF, indicating lower long-term stability. In contrast, matrix "B" and matrix "C" exhibited more gradual reductions in both properties. Specifically, the MOR of matrix "B" and matrix "C" remained relatively stable for up to 85 days, whereas matrix "A" experienced a much faster drop in strength, highlighting the durability benefits of CSA and RFA. For STF, matrix C showed the best performance, with minimal reduction in strength even after extended periods, retaining most of its original STF at around 25 days. Matrix "B" also performed well but showed a slight decline, while matrix "A" exhibited a much faster deterioration, reinforcing its lower long-term durability. Matrix "C" has been considered to study the ageing GRC wire mesh with RFA, and the results are shown in Fig. 22. The incorporation of RFA improved the stability of the matrix and extended the duration over which both MOR and STF remained relatively stable, as shown in Fig. 22a and Fig. 22b.

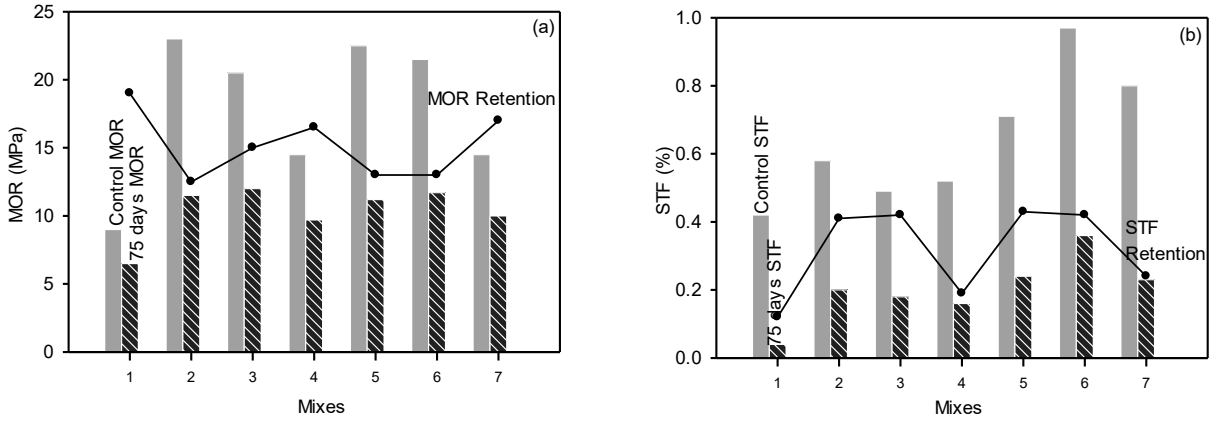

Fig. 22. Effect of ageing: (a) residual MOR after 75 days accelerating ageing, and (b) residual STF after 75 days accelerating ageing.

After 75 days of accelerated ageing, RFA-incorporated mixes retained 50% to 70% of their initial MOR, slightly lower than plain GRC, which retained about 73%. For STF, RFA-GRC with mesh retained 20% to

40% of its initial value, compared to just 12% for unreinforced mixes. This indicates that RFA contributes to both long-term strength and ductility retention in GRC. While increasing the fibre reinforcement improved the initial MOR, it had minimal effect on long-term ductility. The benefits of double-layer reinforcement were limited, as MOR and STF values eventually converged across all mixes. This suggests that fibre mesh reinforcement increases early strength but has a limited impact on maintaining ductility over time. Eventually, RFA improves both MOR and STF retention, enhancing the long-term performance and durability of GRC, especially when combined with fibre mesh reinforcement for better fibre-matrix bonding.

3.6 Development of an enhanced long-term performance durability model of RFA-CSA GRC

As GRC materials gradually degrade over their service life, it is vital for design engineers to determine an appropriate long-term strength value for design purposes. Since extended testing durations are often impractical, this value must be estimated using durability models. For reliable performance, RFA-GRC should be designed based on a simplified design equation that accounts for environmental exposure and material safety, as expressed in Equation (1):

$$f_{GRC,d} = \kappa_{env,t} MOR_{,0} / (\gamma_{GRC}) \quad (1)$$

where $f_{GRC,d}$ is the strength design value, $MOR_{,0}$ is the original bending strength, $\kappa_{env,t}$ (=1/ $\eta_{env,t}$) is the environmental strength retention factor and is the ratio between long-term and original strength, $\eta_{env,t}$ is the strength reduction factor, γ_{GRC} is the material safety factor.

Environmental strength retention factor ($\kappa_{env,t}$) can be determined accurately if the 1000 h strength $f_{fk,1000h}$ a nd the standard reduction of strength per logarithmic decade due to environmental influence R_{10} is adopted . It is expected that there is a shift of about three logarithmic decades from 1000 h to 880,000 h (100 years) or 2.7 logarithmic decades for 50 years life. The following power equation 2 can be used to calculate $\kappa_{env,t}$ (adapted from German Standard (DIN 1990) [44]).

$$\kappa_{env,t} = (1 - R_{10})^n (f_{fk,1000h} / f_{fk,0}) \quad (2)$$

where $f_{fk,0}$ is the original strength, and for normal environmental and service conditions n equals 3.

If no long-term retention factors are known, an estimation using the above approach can be used. Therefore the 1000 h value is determined from short term data of MOR and literature data on strength retention. The following equation was adapted,

$$\kappa_{env,t} = (1 - R_{10})^{n+2} \tag{3}$$

where n is the sum of the different influence terms

$$n = n_T + n_{mo} + n_{SL} \tag{4}$$

where n_T is the term for temperature, n_{mo} is the term for moisture condition (**Error! Reference source not found.**) and n_{SL} is the term for desired service life (n_{SL} = log [time]+1, time in year), typical n_{SL} values according to the desired service life such as 1, 10, 50, 100 years with the values of 1, 2, 2.7, and 3 respectively. The rate of degradation in GRC is significantly influenced by environmental humidity. It has been observed that glass fibres exposed to simulated pore solutions exhibit similar behaviour, with varying impacts depending on the level of humidity. Three distinct humidity conditions are typically identified: dry (approximately 50% relative humidity), moist (around 80% relative humidity), and saturated (close to 100% relative humidity). These conditions have a pronounced accelerating effect on the degradation process. As humidity increases, the rate of deterioration also rises, with higher humidity levels substantially speeding up the degradation of the material, as demonstrated in the accompanying Fig. 23.

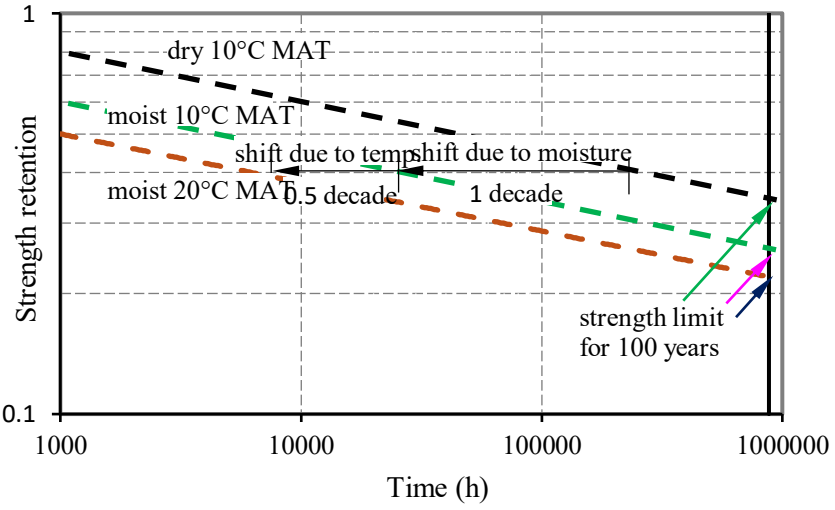

Fig. 23. Effect of the parameter of temperature and humidity on GRC flexural strength retention curves.

4. Proof-of-concept applications: Drainage channel and permanent fence system

Based on the research and optimisation of GRC mix design, two proof-of-concept products like a drainage channel and a permanent fence system were successfully developed using RFA-based GRC. The final formulations were achieved after systematically studying key mix parameters such as water–cement ratio, sand–cement ratio, cementitious materials, and superplasticiser content, ensuring optimal workability and mechanical performance. The selected mix incorporated RFA as a sustainable replacement for natural sand, enhancing matrix compactness and providing improved mechanical interlocking with glass fibres. The fresh-state workability was verified through slump and flow table tests (EN 1170-1, EN 1015-3) [36, 37], confirming balanced fluidity suitable for casting applications. Both the drainage and fence prototypes were produced using casting techniques, following the optimised Technique D, which provided consistent fibre dispersion and uniform matrix quality. The CSA–RFA binder system offered enhanced durability, while the inclusion of SPFA and superplasticiser improved flow without compromising strength. These RFA-GRC products demonstrate the material's potential for sustainable infrastructure applications, validating its practicality for long-term outdoor use and establishing a foundation for further research and commercial development in durable, eco-efficient GRC systems.

4.1 Design and development of drainage channel and permanent formwork

The drainage channel was developed using RFA–GRC mixes and cast using the bottom-up pumping technique to minimize air entrapment, particularly in the thin 12 mm, 1 m-high mould. A modified mould, featuring a 10 × 30 mm inlet slot and a pressure-release guillotine mechanism, allowed smooth material flow, while the PS38A peristaltic pump delivered up to 30 kg/min, ensuring consistent placement. To improve stability and smooth flow, the RFA–GRC mix was enhanced with an anti-foam agent and pump aid. Casting with the bottom-up method achieved excellent compaction and surface finish, with one side of the mould filled within three minutes. This resulted in a nearly flawless finish, as shown in Fig. 24a. In contrast, the top-fill method resulted in numerous air voids near the upper section, highlighting the advantage of the bottom-up technique in achieving better quality. The finished product is shown in Fig.

24b, demonstrating the improved quality and workability achieved using RFA. A lightweight RFA–GRC permanent formwork prototype was developed as a stay-in-place structural element, offering fast installation, strong bonding, and corrosion protection. The unit, which weighed under 30 kg and measured 1.2 m × 1.1 m, had a single corrugated profile, as shown in Fig. 24c. Three mixes with different GRC fibre contents were tested using a timber mould. The plain mix failed during demoulding, while the RFA–GRC mix with fibres showed excellent toughness and surface finish, with minimal air voids. The mould-contact face was smooth, and minor air voids appeared only at the top due to trapped air. These results confirm that RFA–GRC provides sufficient strength, workability, and durability for sustainable permanent formwork applications. The permanent formwork model is shown in Fig. 24d.

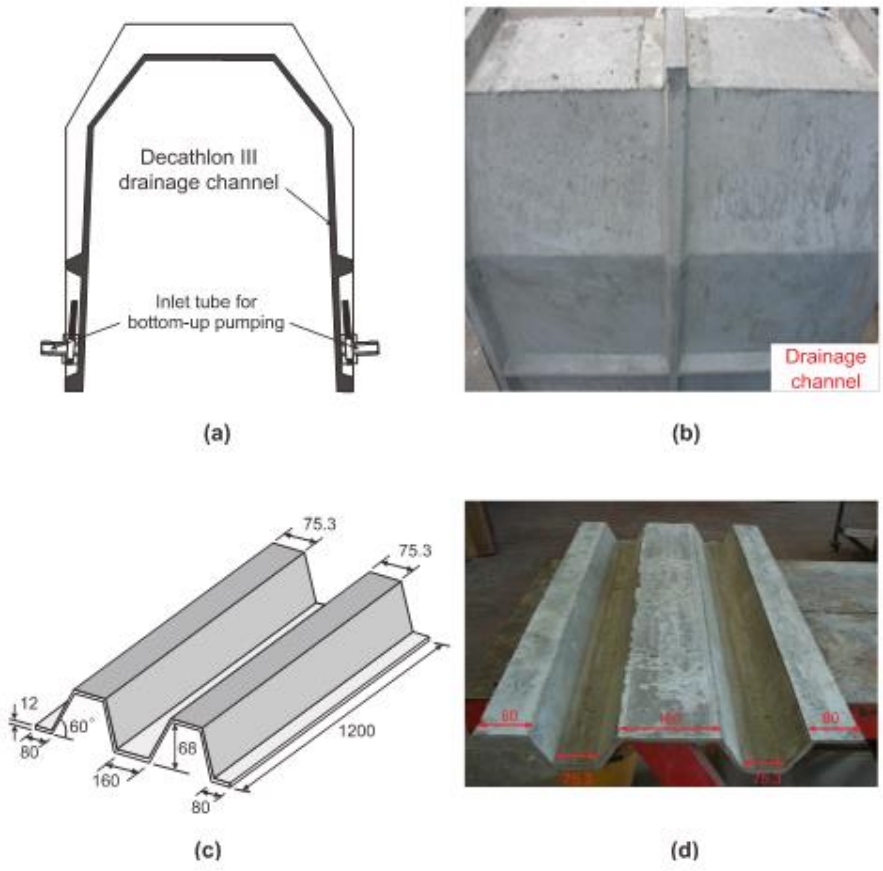

Fig. 24. Proof of concept products: (a) schematic view of drainage channel, (b) channel specimen after casting, (c) schematic view of formwork, and (d) formwork specimen after casting and demoulding.

4.2 Testing programme of the products

The drainage channel, produced using the bottom-up RFA–GRC process, was tested under vertical loading using an Eland 50 kN actuator controlled by a Kelsey Controller. The test was simplified by positioning the unit on its side within a self-reacting frame, supported along the bottom edge. A line load was applied along the upper edge of the channel, simulating service conditions. Three LVDTs were installed to record deflections at the centre, and both ends of the loaded edge. The complete experimental setup for the RFA–GRC drainage channel test is illustrated in Fig. 25a. The RFA–GRC permanent formwork was tested under displacement control, with data recorded using the Orion Data 3530 system. The specimen was simply supported on universal beams spanning 1100 mm, and the load was applied at mid-span via a hydraulic jack through another universal beam. Six LVDTs measured deflection two at mid-span and two at each support. The setup is shown in Fig. 25b. The RFA–GRC fence panels were tested using the same equipment. Each panel was simply supported on rollers and loaded at mid-span through a hydraulic jack. Five LVDTs recorded deflection four at the top corners and one at the bottom centre. The setup is illustrated in Fig. 25b.

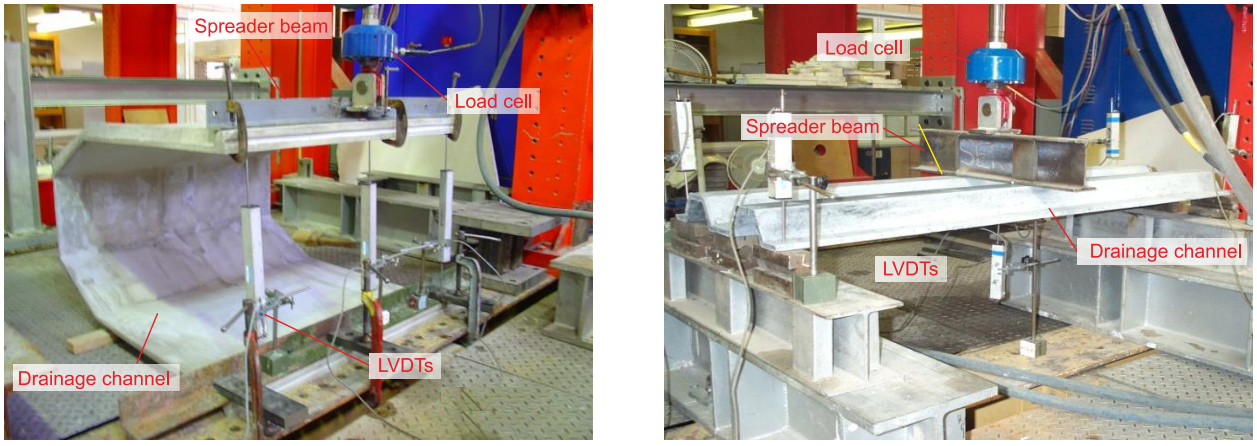

(a) (b)

Fig. 25. Test setup of GRC elements: (a) test setup of drainage channel, (b) test setup of permanent formwork.

4.3 Structural performance of the products

Fig. 26a shows the load-deflection response of the RFA–GRC drainage channel. The initial visible crack appeared at the transition slope along the middle rib when the load reached 0.42 kN. As the load increased,

cracks propagated to the side ribs and extended toward the channel wall. Failure occurred when the wall cracked at the slope junction, corresponding to a peak load of 1.39 kN, accompanied by extensive cracking. This indicates that the RFA–GRC drainage channel exhibited significant resistance to cracking and deformation. The equivalent pressures at first crack and ultimate load were estimated to be 0.0033 MPa and 0.0127 MPa, respectively, showing the unit's strong resistance to hydrostatic pressure. The inclusion of RFA improved the matrix-fibre bond, reducing brittleness and contributing to better crack distribution and energy absorption, as seen in the smoother progression of the load-deflection curve. The RFA mix showed greater energy absorption compared to the conventional mix, and its performance was more consistent under increasing load.

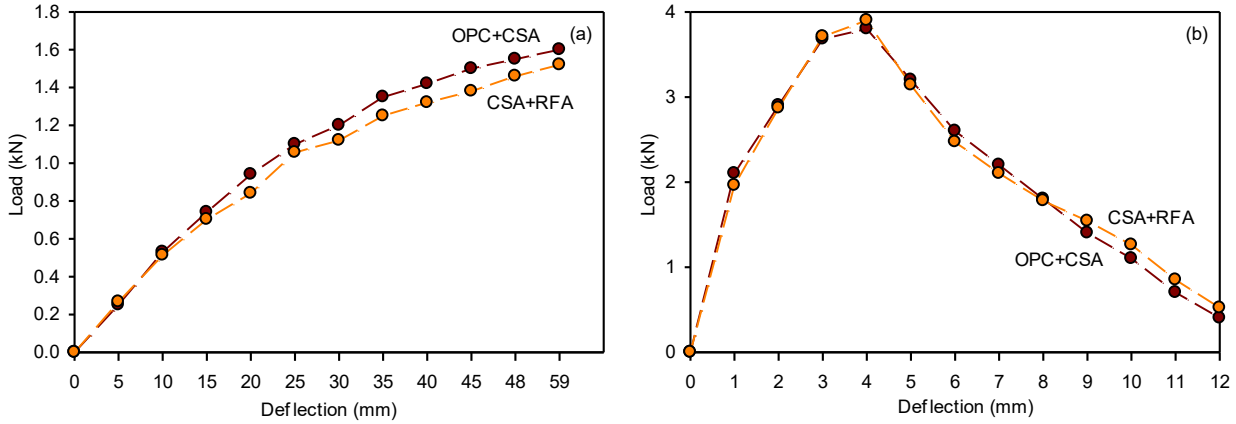

Fig. 26. Load deflection response: (a) load deflection of drainage channel, (b) load deflection of permanent formwork.

The load deflection response of the RFA–GRC permanent formwork is presented in Fig. 26b. The curve starts with a linear portion representing the elastic stage, followed by a gradual deviation as cracking initiates, and stiffness decreases. The formwork exhibited high ductility after the peak, typical of RFA–GRC composites. Fibre bridging across cracks allowed the specimen to sustain increasing loads until peak stiffness was reached, after which softening occurred. The RFA–GRC formwork outperformed the CSA-GRC specimen, with a peak load of 3.98 kN compared to CSA-GRC's 3.74 kN, respectively. For real applications, the smooth side of the RFA–GRC formwork should face upward for aesthetic reasons, while the rough side should face downward to improve bonding with the concrete above. The current horizontal vibration casting method, suitable for short-span elements, resulted in a slightly lower strength for the RFA–

GRC formwork and required extended filling time. This suggests that further optimisation of the casting process is needed to achieve consistent and reliable performance for larger or longer-span applications. The RFA–GRC drainage channel and permanent formwork exhibited superior load capacity, toughness, and ductility compared to CSA-GRC. The incorporation of RFA enhanced the material's ability to absorb energy and resist cracking, making it a promising material for use in structural applications where high performance and durability are essential.

5. Carbon footprint and embodied energy of Low-Carbon GRC materials

The environmental impact of construction materials is a critical aspect in the drive towards sustainable development in the built environment [45, 46]. As the construction industry is responsible for a substantial share of global carbon emissions, understanding and reducing the carbon footprint of materials used in construction is essential [47]. This study explores the carbon footprint and embodied energy associated with the production and use of GRC incorporating CSA cement and RFA. Embodied energy (MJ/kg) and carbon footprint (kg CO_2-e/kg) were estimated for each constituent in the main mix designs (Appendix A.1 and A.2). The reduction in CO_2 emissions when CSA cement is used, compared to OPC, is substantial, with a reduction of 40 to 45% in emissions. By incorporating RFA into the mix, the environmental impact is further minimized, as the need for virgin materials is reduced, and construction waste is diverted from landfills. The environmental benefits of using recycled materials are not only limited to carbon savings but also extend to the reduction in the demand for natural resources, further enhancing the sustainability of the mix.

5.1 Embodied energy of GRC mixes

Embodied energy refers to the total energy required for the production, transportation, and installation of materials [48]. This metric is crucial in evaluating the environmental impact of construction materials [49]. CSA-based GRC, due to the lower energy requirements for CSA cement production, generally exhibits lower embodied energy compared to OPC-based concrete. Table 6 summarizes the carbon footprint (CO_2 emissions) and embodied energy for various GRC mixes, including OPC, CSA, and CSA with RFA. From the results of Table 6, the OPC-based GRC control mix has an embodied energy of 1,300 MJ per m^3 and a

carbon footprint of 1,050 kg CO_2 per m^3.

Table 6. Carbon footprint and embodied energy for various GRC mixes

Mix type	Embodied energy EE (MJ/kg)	Embodied CO_2ECO_{2e} ($kgCO_2/kg$)	Carbon reduction (%)	Energy reduction (%)
OPC	1300	1050	-	-
OPC+CSA	1000	675	35	23
OPC+RFA	900	525	50	31
CSA+RFA	725	350	67	44
OPC+RFA+GRC	850	450	57	35
CSA+RFA+GRC	675	275	74	48

When CSA cement replaces OPC, a 35% reduction in carbon footprint and a 23% reduction in embodied energy are achieved, bringing the values to 675 kg CO_2 and 1,000 MJ per m^3, respectively. The inclusion of RFA further reduces both the carbon footprint and embodied energy, with the OPC + RFA-based GRC showing a 50% reduction in carbon footprint and a 31% reduction in energy, resulting in values of 525 kg CO_2 and 900 MJ per m^3. The CSA + RFA-based GRC mix shows the greatest reductions, with a 67% reduction in carbon emissions and a 44% reduction in embodied energy, reaching 350 kg CO_2 per m^3 and 725 MJ per m^3, respectively. Adding GRC (glass fibre reinforcement) to the OPC + RFA mix results in a 57% reduction in carbon emissions and a 35% reduction in embodied energy, lowering the values to 450 kg CO_2 and 850 MJ per m^3. The most sustainable option, CSA + RFA + GRC, achieves the lowest environmental impact, with 275 kg CO_2 per m^3 and 675 MJ per m^3, marking a 74% reduction in carbon footprint and 48% reduction in embodied energy. These findings confirm that CSA cement and RFA significantly enhance the sustainability of GRC. The major drivers of these reductions are the combined use of CSA cement and RFA, which significantly lower both the energy demand for cement production and the need for virgin raw materials. This approach not only makes the concrete more sustainable but also reduces the overall environmental impact of construction, without compromising the performance of the material.

6. Practical implications and design recommendations

The findings of this study clearly demonstrate that RFA–CSA–GRC composites can be used effectively as sustainable, high-performance materials for a variety of construction applications. The synergy between

RFA, CSA cement, and glass fibres delivers improved early strength, ductility, and long-term durability while significantly reducing the carbon footprint compared with conventional mixes. The self-compacting behaviour achieved through mix optimisation allows for excellent workability and surface finish, making the material ideal for complex shapes and thin-walled elements. The successful production and testing of RFA–GRC drainage channels and permanent formwork confirmed its practical viability, with the bottom-up casting technique effectively eliminating air voids and improving structural integrity. These outcomes illustrate that RFA–GRC not only meets technical requirements but also aligns with circular-economy principles by utilising recycled materials without compromising quality.

For engineering practice, the study proposes a set of design and durability guidelines that can support broader adoption of RFA–CSA–GRC. Designers are encouraged to use 2–3% glass fibre reinforcement and allow up to 100% replacement of natural sand with RFA where suitable. CSA cement should be prioritised for its rapid strength gain and low shrinkage, improving resistance to moisture and chemical attack. For thin or intricate elements, bottom-up or vibration-assisted casting ensures void-free finishes. Structural design should target LOP $\geq$ 4 MPa and MOR $\geq$ 8 MPa, supported by the proposed durability model that integrates environmental retention factors for long-term prediction. Furthermore, given the significant reductions in carbon footprint and embodied energy shown in the study, designers should consider these environmental benefits in their material selection to meet sustainability goals for low-carbon, resilient construction. Eventually, the study provides a foundation for standardising RFA–GRC in prefabricated infrastructure and architectural applications. Future research should focus on full-scale validation, life-cycle analysis, and the development of material design codes to guide implementation in low-carbon, resilient, and circular construction systems.

7. Conclusions and future research

This research comprehensively explored the mechanical behaviour, durability, and practical applicability of RFA–CSA–GRC composites as sustainable alternatives to conventional GRC. Experimental testing, durability analysis, and full-scale prototype development, including drainage channels and permanent

formwork, validated the material's structural performance and long-term stability. The following key conclusions were drawn from this study:

- The compressive strength of RFA and CSA with GRC increased by up to 20% compared with OPC-based mixes, while the elastic modulus showed about 15% improvement, indicating a stiffer and denser matrix.
- RFA–GRC drainage channel prototypes achieved a peak load of 1.59 kN, with an equivalent hydrostatic pressure of 0.01 MPa, confirming adequate structural strength for real-world use.
- Permanent formwork samples of RFA–GRC reached maximum MOR values of 3.77 kN, and LOP of 3.01 kN, demonstrating significant toughness and ductility under service conditions.
- Long-term durability analysis showed RFA and CSA with GRC retained 70 to 80% of original MOR and 40 to 60% of initial STF post-accelerated ageing, outperforming conventional GRC by 30%.
- The environmental retention factor model accurately predicted long-term strength reduction, supporting design ranges for extended lifespans (50–100 years) under typical exposure conditions.
- Addition of SPFA and polymer modifiers improved early-age performance, while RFA contributed to long-term matrix densification and reduced brittleness.
- Full-scale prototype testing confirmed the RFF with GRC viability for prefabricated infrastructure, with lowered weight, reduced cement use, and enhanced sustainability evidenced in field trials.
- RFA with CSA and GRC composites delivered substantial carbon footprint savings (up to 74% reduction, as low as 275 kg CO_2/m^3) and lower embodied energy (up to 48% reduction, with minimum 675 MJ/m^3), making this technology a highly sustainable option for low-carbon construction.

Future work should focus on scaling up RFA–CSA–GRC for industrial production and evaluating its life-cycle performance under real environmental conditions. Advanced numerical modelling should be conducted to simulate crack propagation and long-term degradation. Furthermore, life-cycle analysis

(LCA) and environmental impact assessments should be prioritized to assess the carbon footprint and embodied energy of RFA–CSA–GRC in different construction applications, ensuring that the material's sustainability benefits are fully quantified. Developing standardised mix design protocols, durability classification systems, and design codes for RFA–GRC would accelerate its implementation in low-carbon construction. Further optimisation of fibre type, RFA gradation, and curing conditions is also recommended to achieve maximum performance and consistency in full-scale manufacturing.

Acknowledgements

This research was funded by National Research Council of Thailand (N42A680074).

References

[1] Guo, Y., Luo, L., Liu, T., Hao, L., Li, Y., Liu, P. and Zhu, T., 2024. A review of low-carbon technologies and projects for the global cement industry. Journal of Environmental Sciences, 136, pp.682-697. https://doi.org/10.1016/j.jes.2023.01.021.

[2] Kothari, A., Tole, I., Hedlund, H., Ellison, T. and Cwirzen, A., 2023. Partial replacement of OPC with CSA cements–effects on hydration, fresh and hardened properties. Advances in Cement Research, 35(5), pp.207-224. https://doi.org/10.1680/jadcr.22.00054.

[3] Hossein, H.A., Nabawy, B.S., Sanad, S.A. and El-Alfi, E.A., 2025. Manufacturing of high-quality green CSA-supported OPC cement with optimum physical and mechanical properties. Scientific Reports, 15(1), p.29158. https://doi.org/10.1038/s41598-025-14008-w.

[4] Kwan, A.K.H. and Ling, S.K., 2017. Filler technology for improving robustness and reducing cementitious paste volume of SCC. Construction and Building Materials, 153, pp.875-885. https://doi.org/10.1016/j.conbuildmat.2017.07.160.

[5] Figueiras, H., Nunes, S., Coutinho, J.S. and Andrade, C., 2014. Linking fresh and durability properties of paste to SCC mortar. cement and concrete composites, 45, pp.209-226. https://doi.org/10.1016/j.cemconcomp.2013.09.020.

[6] Gheidan, E., Ab. Kadir, M.A. and Aluko, O.G., 2025. A thorough review of thermal and mechanical properties of fiber-reinforced ordinary Portland cement-SCC and pozzolanic-SCC. Journal of Structural Fire Engineering, 16(2), pp.268-290. https://doi.org/10.1108/JSFE-08-2024-0031.

[7] Akerele, D.D. and Aguayo, F., 2024. Evaluating the Impact of CO2 on Calcium SulphoAluminate (CSA) Concrete. Buildings, 14(8), p.2462. https://doi.org/10.3390/buildings14082462.

[8] Karataş, M., Benli, A. and Ergin, A., 2017. Influence of ground pumice powder on the mechanical properties and durability of self-compacting mortars. *Construction and Building Materials*, *150*, pp.467-479. https://doi.org/10.1016/j.conbuildmat.2017.05.220.

[9] Benli, A., Karatas, M. and Toprak, H.A., 2020. Mechanical characteristics of self-compacting mortars with raw and expanded vermiculite as partial cement replacement at elevated temperatures. *Construction and Building Materials*, *239*, p.117895. https://doi.org/10.1016/j.conbuildmat.2019.117895.

[10] Benli, A., Karatas, M. and Toprak, H.A., 2020. Mechanical characteristics of self-compacting mortars with raw and expanded vermiculite as partial cement replacement at elevated temperatures. *Construction and Building Materials*, *239*, p.117895. https://doi.org/10.1016/j.conbuildmat.2019.117895.

[11] Sarac, S., Karatas, M. and Benli, A., 2023. The effect of dunite powder and silica fume on the viscosity, physico-mechanical properties and sulphate resistance of self-compacting mortars. *Construction and Building Materials*, *375*, p.130970. https://doi.org/10.1016/j.conbuildmat.2023.130970.

[12] Chen, H., Wang, P., Pan, J., Lawi, A.S. and Zhu, Y., 2021. Effect of alkali-resistant glass fiber and silica fume on mechanical and shrinkage properties of cement-based mortars. Construction and Building Materials, 307, p.125054. https://doi.org/10.1016/j.conbuildmat.2021.125054.

[13] Ibrahim, H., Wardeh, G., Fares, H. and Ghorbel, E., 2025. Mechanical and fracture properties of mortars reinforced with glass fibre and prepared with different cement types. *International Journal of Building Pathology and Adaptation*, *43*(4), pp.712-731. https://doi.org/10.1108/IJBPA-12-2023-0197.

[14] Kaplan, G., Coskan, U., Benli, A., Bayraktar, O.Y. and Kucukbaltacı, A.B., 2021. The impact of natural and calcined zeolites on the mechanical and durability characteristics of glass fiber reinforced cement composites. *Construction and Building Materials*, *311*, p.125336. https://doi.org/10.1016/j.conbuildmat.2021.125336.

[15] Benli, A., 2024. Sustainable use of waste glass sand and waste glass powder in alkali-activated slag foam concretes: Physico-mechanical, thermal insulation and durability characteristics. *Construction and Building Materials*, *438*, p.137128. https://doi.org/10.1016/j.conbuildmat.2024.137128.

[16] Imjai, T., Sridhar, R., Leelatanon, S., Setkit, M., Ghorbel, E. and Kim, B., 2025. High performance synthetic fiber-reinforced concrete mixed with nanoparticles: A proof-of-concept green railway sleeper product. Sustainable Structures, 5(1). https://doi.org/10.54113/j.sust.2025.000066.

[17] Lotfy, A. and Al-Fayez, M., 2015. Performance evaluation of structural concrete using controlled quality coarse and fine recycled concrete aggregate. Cement and concrete composites, 61, pp.36-43. https://doi.org/10.1016/j.cemconcomp.2015.02.009.

[18] Park, S., Jeong, Y., Moon, J. and Lee, N., 2021. Hydration characteristics of calcium sulfoaluminate (CSA) cement/portland cement blended pastes. *Journal of Building Engineering*, *34*, p.101880. https://doi.org/10.1016/j.jobe.2020.101880.

[19] Ali, B. and Qureshi, L.A., 2019. Influence of glass fibers on mechanical and durability performance of concrete with recycled aggregates. *Construction and Building Materials*, *228*, p.116783. https://doi.org/10.1016/j.conbuildmat.2019.116783.

[20] Ali, B., Qureshi, L.A., Shah, S.H.A., Rehman, S.U., Hussain, I. and Iqbal, M., 2020. A step towards durable, ductile and sustainable concrete: Simultaneous incorporation of recycled aggregates, glass fiber and fly ash. *Construction and Building Materials*, *251*, p.118980. https://doi.org/10.1016/j.conbuildmat.2020.118980.

[21] Zhang, F., Lu, Z. and Wang, D., 2024. Working and mechanical properties of waste glass fiber reinforced self-compacting recycled concrete. *Construction and Building Materials*, *439*, p.137172. https://doi.org/10.1016/j.conbuildmat.2024.137172.

[22] Dehghan, A., Peterson, K. and Shvarzman, A., 2017. Recycled glass fiber reinforced polymer additions to Portland cement concrete. *Construction and Building Materials*, *146*, pp.238-250. https://doi.org/10.1016/j.conbuildmat.2017.04.011.

[23] Baena, M., Torres, L., Turon, A., Llorens, M. and Barris, C., 2016. Bond behaviour between recycled aggregate concrete and glass fibre reinforced polymer bars. Construction and Building Materials, 106, pp.449-460. https://doi.org/10.1016/j.conbuildmat.2015.12.145.

[24] Raza, A., Rashedi, A., Rafique, U., Hossain, N., Akinyemi, B. and Naveen, J., 2021. On the structural performance of recycled aggregate concrete columns with glass fiber-reinforced composite bars and hoops. *Polymers*, *13*(9), p.1508. https://doi.org/10.3390/polym13091508.

[25] Abellan-Garcia, J., Khan, M.I., Abbas, Y.M., Martínez-Lirón, V. and Carvajal-Muñoz, J.S., 2023. The drying shrinkage response of recycled-waste-glass-powder-and calcium-carbonate-based ultrahigh-performance concrete. *Construction and Building Materials*, *379*, p.131163. https://doi.org/10.1016/j.conbuildmat.2023.131163.

[26] Bayraktar, O.Y., Yakupoglu, U. and Benli, A., 2023. Slag/diatomite-based alkali-activated lightweight composites containing waste andesite sand: mechanical, insulating, microstructural and durability properties. *Archives of Civil and Mechanical Engineering*, *23*(4), p.230. https://doi.org/10.1007/s43452-023-00774-9.

[27] Bodur, B., Benli, A., Bayraktar, O.Y., Alcan, H.G., Kaplan, G. and Aydın, A.C., 2025. Impact of attapulgite and basalt fiber additions on the performance of pumice-based foam concrete: mechanical, thermal, and durability properties. *Archives of Civil and Mechanical Engineering*, *25*(2), p.74. https://doi.org/10.1007/s43452-025-01128-3.

[28] Dener, M., Altunhan, U. and Benli, A., 2024. A green binder for cold weather applications: enhancing mechanical performance of alkali-activated slag through modulus, alkali dosage, and Portland cement substitution. *Archives of Civil and Mechanical Engineering*, *24*(3), p.176. https://doi.org/10.1007/s43452-024-00991-w.

[29] Koksal, F., Nazlı, T., Benli, A., Gencel, O. and Kaplan, G., 2021. The effects of cement type and expanded vermiculite powder on the thermo-mechanical characteristics and durability of lightweight mortars at high temperature and RSM modelling. *Case Studies in Construction Materials*, *15*, p.e00709. https://doi.org/10.1016/j.cscm.2021.e00709.

[30] British Standards Institution (2011) BS EN 197-1:2011 - Cement - Part 1: Composition, specifications, and conformity criteria for common cements, London: BSI.

[31] Arslan, S., Öz, A., Benli, A., Bayrak, B., Kaplan, G. and Aydın, A.C., 2024. Sustainable use of silica fume and metakaolin in slag/fly ash-based self-compacting geopolymer composites: Fresh, physico-mechanical and durability properties. *Sustainable Chemistry and Pharmacy*, *38*, p.101512. https://doi.org/10.1016/j.scp.2024.101512.

[32] ASTM International (2011) ASTM C311/C311M-11. Standard test methods for sampling and testing fly ash or natural pozzolans for use in Portland-cement concrete, West Conshohocken, PA: ASTM International.

[33] ASTM International (1989) ASTM D3379-75. Standard Test Method for Tensile Strength and Young's Modulus for High-Strength Single Filament Materials, West Conshohocken, PA: ASTM International.

[34] Bayraktar, O.Y., Yarar, G., Benli, A., Kaplan, G., Gencel, O., Sutcu, M., Kozłowski, M. and Kadela, M., 2023. Basalt fiber reinforced foam concrete with marble waste and calcium aluminate cement. *Structural Concrete*, *24*(1), pp.1152-1178. https://doi.org/10.1002/suco.202200142.

[35] Benli, A., Bayraktar, O.Y., Karataş, M., Bodur, B., Yılmazoğlu, M.U. and Kaplan, G., 2025. Dunite powder as a green precursor in one-part alkali-activated composites: Effects on mechanical and durability properties. *Sustainable Chemistry and Pharmacy*, *44*, p.101964. https://doi.org/10.1016/j.scp.2025.101964.

[36] BS EN 1170-1:1998 (1998) *Precast concrete products – Test method for glass-fibre-reinforced cement – Part 1: Measuring the consistency of the matrix ('Slump test' method)*. London: British Standards Institution.

[37] European Committee for Standardization (CEN) (1999) EN 1015-3:1999 Methods of test for mortar for masonry – Part 3: Determination of consistence of fresh mortar (by flow table). Brussels: CEN.

[38] EFNARC (2001) Specification for Polymer-Modified Cementitious Flooring as Wearing Surfaces for Industrial and Commercial Use. Farnham: EFNARC.

[39] Bayraktar, O.Y., Bozkurt, T.H., Benli, A., Koksal, F., Türkoğlu, M. and Kaplan, G., 2023. Sustainable one-part alkali activated slag/fly ash Geo-SIFCOM containing recycled sands: Mechanical, flexural, durability and microstructural properties. *Sustainable Chemistry and Pharmacy*, *36*, p.101319. https://doi.org/10.1016/j.scp.2023.101319.

[40] CEN (2002) EN 12390-3:2002 Testing hardened concrete – Part 3: Compressive strength of test specimens. Brussels: European Committee for Standardization.

[41] CEN (1997) EN 1170-5:1997 Precast concrete products – Test method for glass-fibre reinforced cement – Part 5: Measuring bending strength, "Complete bending test" method. Brussels: European Committee for Standardization.

[42] Vinoth, G., Moon, S.W., Moon, J. and Ku, T., 2018. Early strength development in cement-treated sand using low-carbon rapid-hardening cements. *Soils and Foundations*, *58*(5), pp.1200-1211. https://doi.org/10.1016/j.sandf.2018.07.001.

[43] Huang, G., Pudasainee, D., Gupta, R. and Liu, W.V., 2019. Hydration reaction and strength development of calcium sulfoaluminate cement-based mortar cured at cold temperatures. Construction and Building Materials, 224, pp.493-503. https://doi.org/10.1016/j.conbuildmat.2019.07.085.

[44] DIN (1990). Extrapolation method for the prediction of the long-term behaviour. Berlin, Beuth Verlag.

[45] Lei, B., Yu, L., Chen, Z., Yang, W., Deng, C. and Tang, Z., 2022. Carbon emission evaluation of recycled fine aggregate concrete based on life cycle assessment. *Sustainability*, *14*(21), p.14448. https://doi.org/10.3390/su142114448.

[46] Barbhuiya, S., Das, B.B., Adak, D., Kapoor, K. and Tabish, M., 2025. Low carbon concrete: Advancements, challenges and future directions in sustainable construction. *Discover Concrete and Cement*, *1*(1), pp.1-24. https://doi.org/10.1007/s44416-025-00002-y.

[47] Anderson, J. and Moncaster, A., 2020. Embodied carbon of concrete in buildings, Part 1: analysis of published EPD. *Buildings & Cities*, *1*(1). https://doi.org/10.5334/bc.59.

[48] Zapata, J.F., Azevedo, A., Fontes, C., Monteiro, S.N. and Colorado, H.A., 2022. Environmental impact and sustainability of calcium aluminate cements. *Sustainability*, *14*(5), p.2751. https://doi.org/10.3390/su14052751.

[49] Estrada, H. and Lee, L., 2023. Embodied energy and carbon footprint of concrete compared to other construction materials. *Athens Journal of Technology & Engineering*, *10*(2), p.107. https://doi.org/10.30958/ajte_v10i2.

Appendix A: Mix designations and details of OPC, CSA cement with RFA and GRC

Appendix A.1. Mix details of OPC, CSA cement with the addition of RFA and glass fibres

Mix	RFA/Cement	Water/ Cement	Water/dry materials	Fibre (%)	Workability approaches		
					1 (mm)	2 (mm)	3 (Sec)
1a	0.500	0.45	0.3	4.5	135	190	9.0
1b				6.0	135	180	10.0
2a	0.625	0.45	0.28	4.9	130	190	11.0
2b				6.0	125	180	12.5
3a	0.750	0.45	0.26	5.3	120	185	13.0
3b				6.0	125	180	14.0
4a	0.875	0.45	0.24	5.6	115	185	14.5
4b				6.0	85	175	16.0
5a	1.000	0.45	0.22	6.0	95	170	15.5
5b				6.0	95	160	16.0
5c				6.0	65	150	16.0

Appendix A.2. Effect of white Portland cement using RFA on workability

Mix	White cement	SPFA	RFA	Water	SP (%)	Fibre (%)	Workability approaches (mm)		
							1 (mm)	2 (mm)	3 (Sec)
1	100	-	70	45	-	3	70	115	9.0
2	100	-	70	30	0.3	3	65	80	10.0
3	100	-	70	30	0.6	3	115	135	11.0
4	100	-	70	30	1.0	3	140	180	12.5
5	70	30	70	30	0.5	3	110	135	14.5
6	70	30	70	30	1.0	3	167	187	16.5
7	80	20	60	30	0.8	3	125	160	14.0
8	90	10	70	35	0.5	4	140	175	15.0
9	100	10	50	40	1.2	3	155	180	16.0
10	80	20	50	45	0.4	4	120	150	18.0

Appendix A.3. Mix design and flow time of SCC mixes with RFA and GRC

Fibre type (%)	Initial flow time (Sec)	Final flow time (Sec)	GRC flow time (Sec)	Flow performance
X-1000 (2%)	12.7	12.5	27.5	Good
X-1000 (2.5%)	13.0	14.4	85.1	Moderate
X-1000 (3%)	12.1	14.1	22.4	Good
X-1000 (3.5%)	11.7	13.0	18.2	Good
EF-500 (2%)	13.0	14.4	85.1	Moderate
EF-500 (2.5%)	14.0	15.0	90.2	Moderate
EF-500 (3%)	13.5	14.2	70.0	Moderate
EF-500 (3.5%)	12.0	12.8	60.5	Moderate
MF-2000 (2%)	21.3	22.1	40.6	Low
MF-2000 (2.5%)	22.5	23.0	50.2	Low
MF-2000 (3%)	23.0	23.5	55.0	Low
MF-2000 (3.5%)	25.0	25.0	65.4	Low
UF-300 (2%)	53.8	53.8	75.0	Very low
UF-300 (2.5%)	55.0	55.0	90.0	Very low
UF-300 (3%)	57.3	57.3	95.0	Very low
UF-300 (3.5%)	60.0	60.0	101.6	Very low
SF-800 (2%)	17.2	17.2	41.9	Moderate
SF-800 (2.5%)	18.0	18.0	50.2	Moderate
SF-800 (3%)	18.5	18.5	55.5	Moderate
SF-800 (3.5%)	19.0	19.0	60.3	Moderate

Note: X-1000 represents high strength fibre, EF represents eco-friendly fibres, MF represents macro synthetic based poly fibre, UF represents ultra-fine fibre, and SF represents high-performance fibre.

Appendix B: Compression strength performance of OPC, CSA cement with RFA and GRC

Appendix B.1. Compressive strength results of CSA with RFA in GRC

CSA	SPFA	NFA or RFA	Water	SP	Fibre	Strength (MPa)	STDV (MPa)
100	-	70-NFA	30	0.8	-	67.4	3.5
100	-	70-NFA	30	0.8	17 (1%)	66.7	3.2
100	-	70-NFA	30	0.8	34 (2%)	65.6	2.8
85	15	70-NFA	30	0.8	34 (2%)	61.1	2.9
70	30	70-NFA	30	0.8	34 (2%)	60.2	3.2
100	-	70-NFA	30	0.8	51 (3%)	64.7	3.9
100	-	70-NFA	30	0.8	68 (4%)	64.2	2.3
100	-	70-RFA	30	0.9	17 (1%)	63.7	3.3
95	05	70-RFA	30	0.9	34 (2%)	62.8	3.1
90	10	70-RFA	30	1.0	34 (2%)	62.1	2.7
85	15	70-RFA	30	1.0	51 (3%)	58.7	2.5
70	30	70-RFA	30	1.0	68 (4%)	56.4	2.1

Appendix C: Flexural strength performance of OPC, CSA cement with RFA and GRC

Appendix C.1: Computer program developed in Compaq Visual FORTRAN 6.6

```
! Average of test results
        implicit none
        integer :: NumOfTest
        integer :: DataLength
        integer :: i,j,k
        real,allocatable  :: V(:)
        character(len=10) :: Fin, Fout
        write (*,*) "Please input the number of tests carried out:"
        read (*,*) NumOfTest
        write (*,*) "Please input the length of data array:"
        read (*,*) Fin
        write (*,*) "Please input the output data file name"
        read (*,*) Fout
                do i=1, DataLength
                if (.not. Eof(20)) then
                        read (20, *) V(1:NumOfTest)
                        print *, V
                        k=0
                        Sum=0
                        do j=1,NumOfTest
                                if (V(j)/=0) then
                                        k=k+1
                                        Sum=Sum+V(j)
                                end if
                        end do
                        if (k/=0) then
                                write (21, '(F8.3)') Sum/k
                        end if
                else
                        exit
                end if
        end do
        close(20)
        close(21)
        stop
end
```

Appendix C.2: Model load deflection curves of bending test

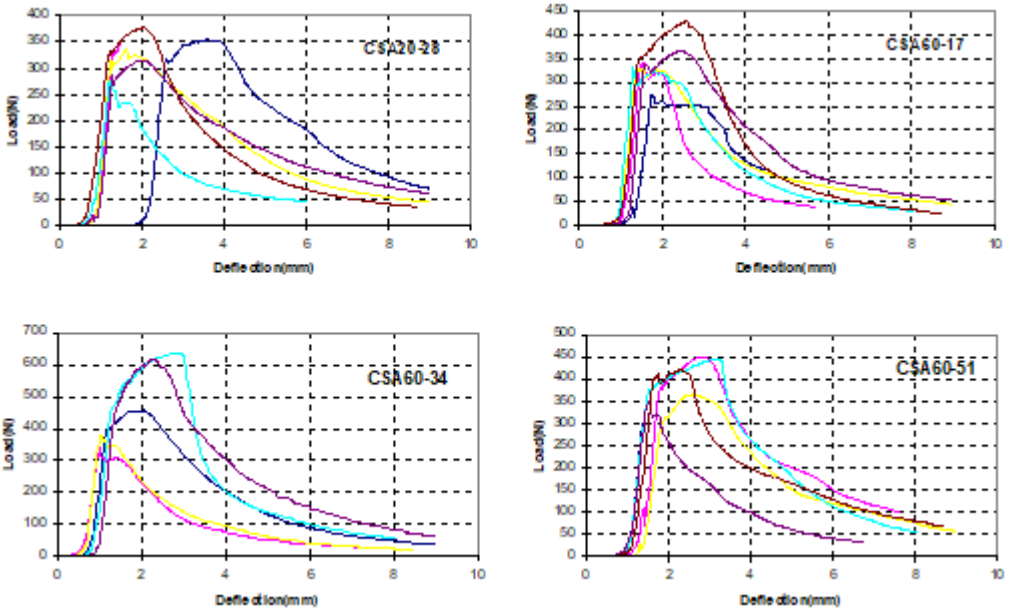

Appendix C.3: Histogram with fitted probability distribution plot for find out modulus of elasticity

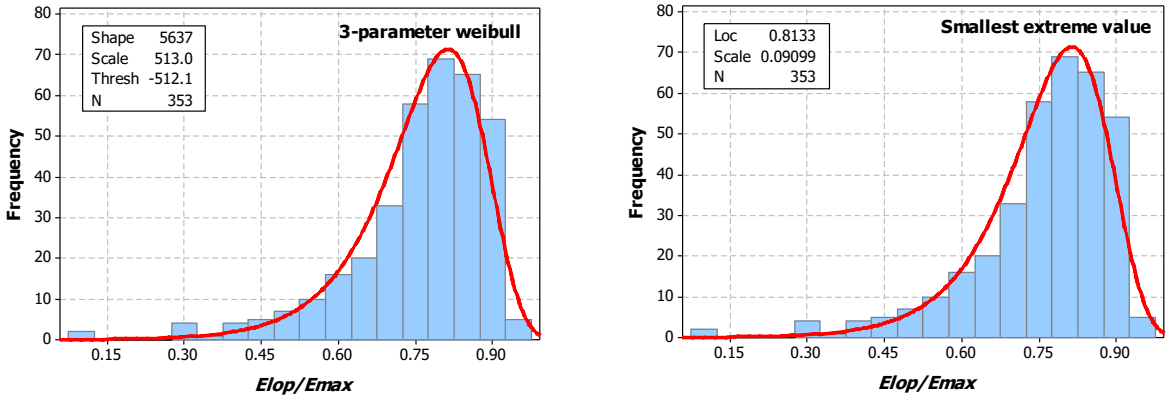

Appendix C.4: Probability plot with 95% confidence level

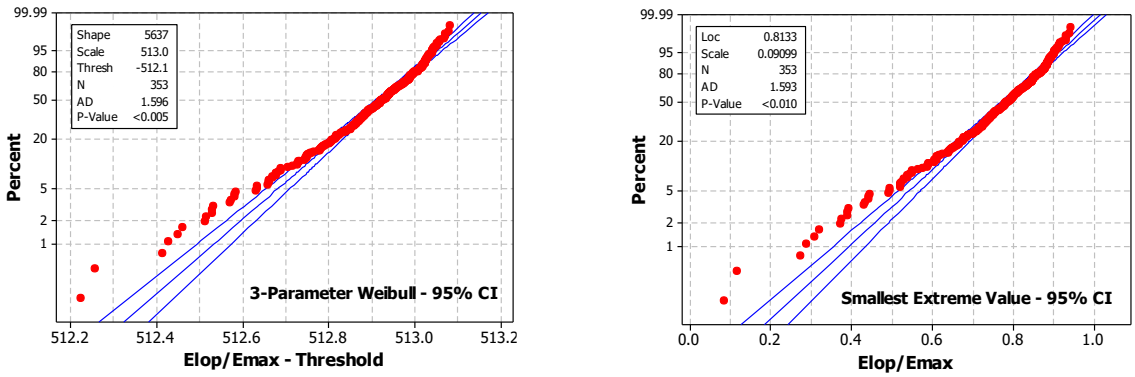

Appendix D: Bond strength performance of OPC, CSA cement with RFA and GRC

Appendix D.1. Bond strength results of CSA with RFA in GRC

Group	Length (l) (mm)	Ageing temp. (°C)	Ageing time (days)	Peak load (N)	Tensile σ (MPa)	Average bond (τ) (MPa)	Standard deviation (MPa)
1	4	20	28	15.0	153.4	0.60	0.10
2	4	28	28	14.7	150.3	0.59	0.07
3	6	28	7	19.0	194.3	0.51	0.06
4	6	28	7	18.7	191.2	0.50	0.05
5	6	38	14	17.0	173.8	0.46	0.04
6	8	38	60	26.3	268.9	0.53	0.05
7	10	20	150	38.0	388.5	0.61	0.09
8	6	20	28	23.0	235.2	0.62	0.06

Appendix D.2. Bond slip behaviour results of CSA with RFA in GRC

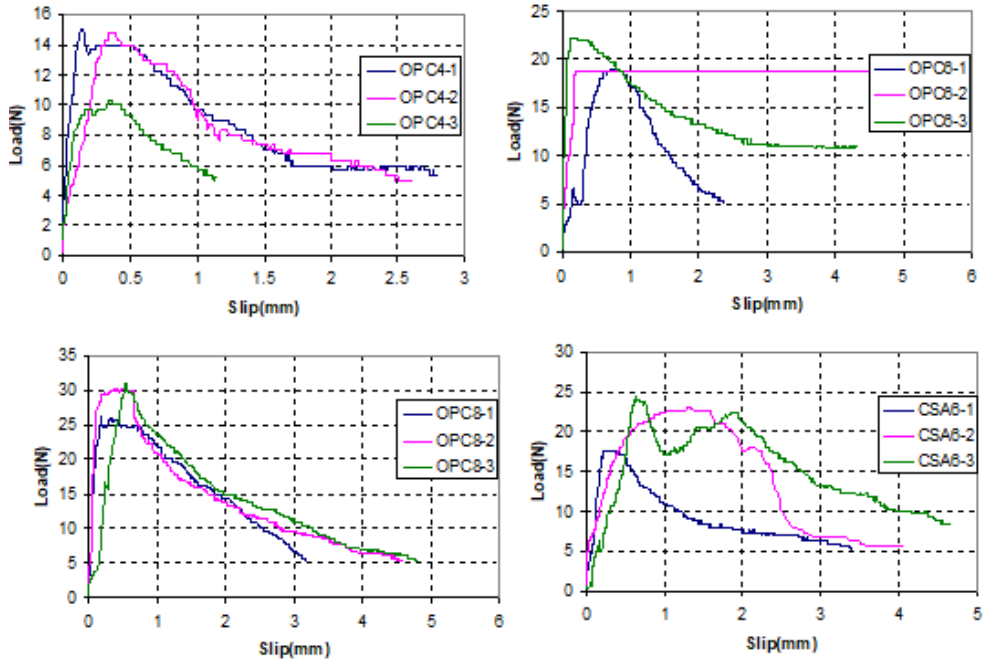

Appendix E: Long-term performance of OPC, CSA cement with RFA and GRC

Appendix E.1. Time dependent performance of different matrices with the incorporation of OPC, CSA, RFA, GRC

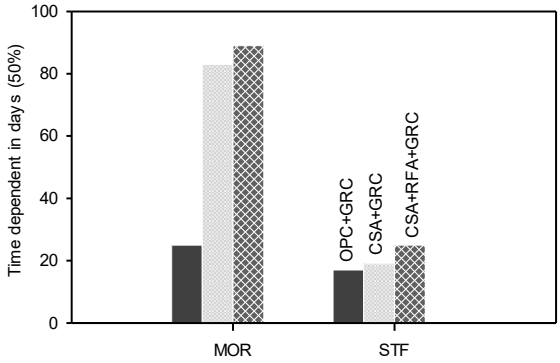

Appendix E.2. Influence of fibre content, length, and type on LOP and MOP

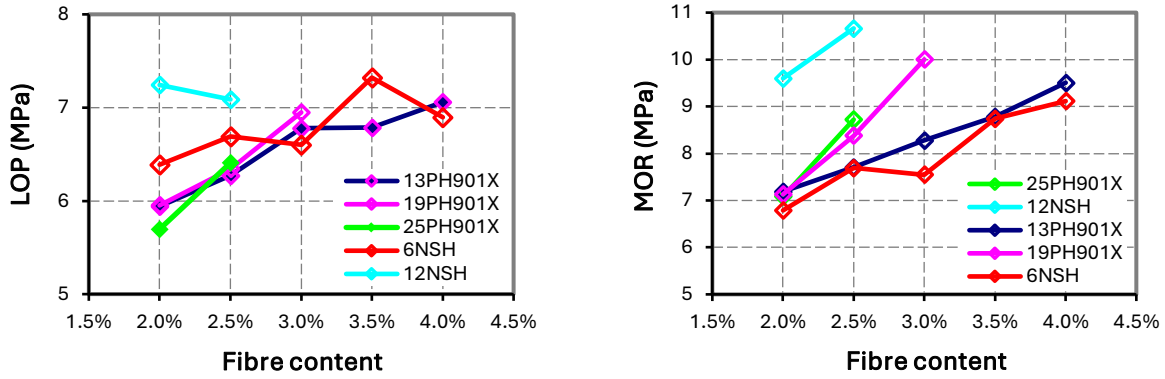

Appendix E.3. Influence of fibre content, filament diameter, and strand integrity on LOP and MOP

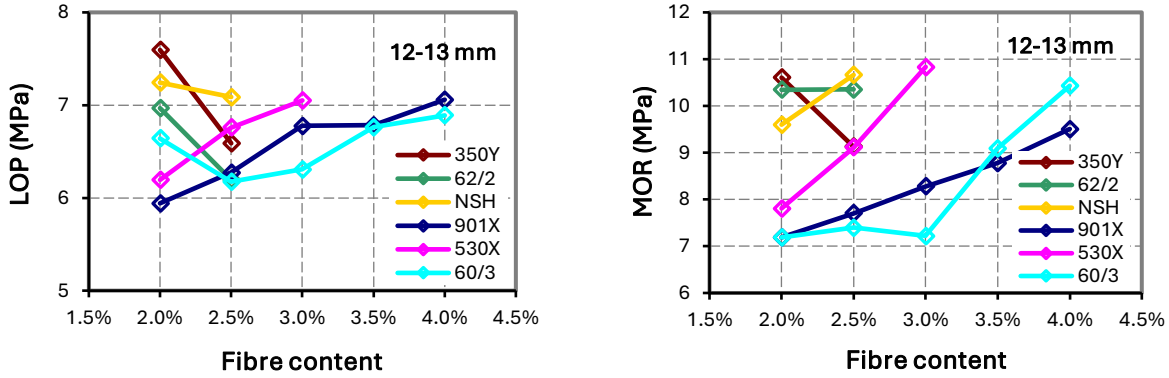

Appendix E.4. Ageing test results of GRC wire mesh with RFA

Age of sample (days)	Measured parameters	Specimens						
		1	2	3	4	5	6	7
10	LOR (MPa)	7.70	7.75	8.45	7.90	8.45	7.65	8.95
	MOR (MPa)	8.45	9.00	8.50	8.70	9.00	10.00	8.30
	STF (%)	0.35	0.95	0.55	0.60	0.60	1.05	0.70
20	LOR (MPa)	7.70	7.75	8.40	8.10	7.80	7.80	7.70
	MOR (MPa)	18.50	16.00	18.30	14.60	7.70	9.90	8.40
	STF (%)	0.30	0.28	0.55	0.60	0.47	0.45	0.75
30	LOR (MPa)	7.10	7.15	7.60	7.90	7.75	7.65	7.60
	MOR (MPa)	7.65	7.95	15.50	8.50	7.70	8.40	7.80
	STF (%)	0.22	0.26	0.33	0.27	0.29	0.50	0.63
40	LOR (MPa)	6.80	6.80	7.00	6.90	6.95	7.30	7.10
	MOR (MPa)	13.50	13.80	9.20	10.20	7.30	7.80	8.40
	STF (%)	0.12	0.72	0.35	0.70	0.43	0.45	0.50
45	LOR (MPa)	6.75	11.20	6.70	5.90	6.85	6.55	6.10
	MOR (MPa)	11.50	12.60	9.00	8.50	8.65	9.20	6.80
	STF (%)	0.08	0.47	0.42	0.52	0.31	0.49	0.35
60	LOR (MPa)	6.60	6.15	6.55	6.80	6.60	6.90	6.80
	MOR (MPa)	11.80	11.50	9.90	10.30	10.00	9.60	8.90
	STF (%)	0.38	0.43	0.41	0.43	0.40	0.36	0.42
75	LOR (MPa)	7.50	8.40	8.20	8.60	8.80	9.10	8.85
	MOR (MPa)	8.90	22.80	19.70	8.90	21.80	21.00	14.60
	STF (%)	0.43	1.20	1.55	1.05	1.30	1.50	0.90